

University of Southern Queensland
Faculty of Health, Engineering & Sciences

Optimisation of an electric powered air-gliding skateboard

A dissertation submitted by

Benjamin Allan John

in fulfilment of the requirements of

ENG4111 & ENG4112 – Research Project Parts 1&2

towards the degree of

Bachelor of Engineering (Mechanical)

Submitted: October 30th, 2014

Abstract

This study aims to improve the design of a novel air gliding skateboard hoverboard that operates on a cushion of air. It aims to achieve this by reducing the system pressure losses through optimisation of 4 key parameters.

The parameters affecting pressure losses through the system are reduced by Buckingham's Pi Theorem to 5 dimensionless Pi Groups which form the basis of a Computational Fluid Dynamics study. This study uses 21 Simulations to define the key relationships between each of the Dimensionless Pi Groups and to propose the optimum skirt configuration for reducing pressure losses. Valid power and flow rate inputs for the CFD study are experimentally determined from an Ozito OZBL 1800WA Leaf Blower.

The optimum skirt configuration is found to be 50 outlet holes 0.009m in diameter spaced evenly at 0.0675 m from the centreline of the skirt. The optimum inlet velocity was specified as 4.06 m/s.

These results determined that through optimisation of the pressure losses through the skirt the power requirements can be reduced and the height of the air cushion increased. This study will form the basis of experimental validation of the CFD model and lead to the eventual creation of a marketable hoverboard.

University of Southern Queensland
Faculty of Health, Engineering and Sciences

ENG4111 /ENG4112 <i>Research Project</i>

Limitations of Use

The Council of the University of Southern Queensland, its Faculty of Health, Engineering & Sciences, and the staff of the University of Southern Queensland, do not accept any responsibility for the truth, accuracy or completeness of material contained within or associated with this dissertation.

Persons using all or any part of this material do so at their own risk, and not at the risk of the Council of the University of Southern Queensland, its Faculty of Health, Engineering & Sciences or the staff of the University of Southern Queensland.

This dissertation reports an educational exercise and has no purpose or validity beyond this exercise. The sole purpose of the course pair entitled “Research Project” is to contribute to the overall education within the student’s chosen degree program. This document, the associated hardware, software, drawings, and other material set out in the associated appendices should not be used for any other purpose: if they are so used, it is entirely at the risk of the user.

Dean

Faculty of Health, Engineering and Sciences

Certification of Dissertation

I certify that the ideas, designs and experimental work, results, analysis and conclusions set out in the dissertation are entirely my own efforts except where otherwise indicated and acknowledged.

I further certify that the work is original and has not been previously submitted for assessment in any other course or institution, except where specifically stated.

BENJAMIN ALLAN JOHN

Student Number: 0050057730

Signature

Date

Acknowledgements

I would like to give acknowledgement to the following people:

Dr Ruth Mossad for her supervision and guidance.

Andrew Tuxford for his assistance with experimental testing.

Greg Valler and Brett Salomon for reviewing my work.

Patrick Taylor for his help with CFX simulation.

To my wife Sarah who has patiently supported me over the last 5 years of study.

Without her support, I would not be where I am today.

BENJAMIN JOHN

University of Southern Queensland

October 2014

Contents

Abstract	i
Certification of Dissertation	iii
Acknowledgements	iv
List of Figures	x
List of Tables	xiii
Nomenclature and Acronyms	xiv
Chapter 1 Introduction	1
1.1 Background	1
1.2 Outline of the Study	1
1.3 Problem Outline	2
1.4 Research Objectives	3
1.5 Methodology Summary	5
1.6 Project Contributions	6

1.7	Consequential Effects	6
1.8	Dissertation Outline	8
1.8.1	Chapter 2 – Literature Review	8
1.8.2	Chapter 3 – Methodology	8
1.8.3	Chapter 4 – Results and Discussion	8
1.8.4	Chapter 5 – Further Work	9
1.8.5	Chapter 6 – Conclusions	9
1.9	Summary	9
Chapter 2 Literature Review		10
2.1	Ionocraft	10
2.2	Magnetic Levitation	12
2.3	Air Operated	14
2.3.1	Hovercraft	14
2.3.2	Air-Gliding Skateboards	17
2.4	Dimensional Analysis	19
Chapter 3 Methodology		21
3.1	Key Design Constraints	22
3.1.1	Minimum Pressure Requirement	22
3.1.2	Validation of Commercial Leaf Blower	25

3.1.3	Leaf Blower Validation results	28
3.1.4	CFD Parameters	31
3.1.5	Summary	35
3.2	Dimensional Analysis	35
3.2.1	Buckingham Pi Theorem	36
3.2.2	Defining Pi Groups	36
3.2.3	Summary	38
3.3	CFD Simulation	38
3.3.1	3-D Model	38
3.3.2	Meshing Structure	40
3.3.3	Fluid Properties	42
3.3.4	Boundary Conditions	42
3.3.5	Simulation Solver	46
3.3.6	Post Processing Simulation Data	48
3.3.7	Model Validation	49
3.3.8	Limitations of Use	49
3.4	Summary	50
Chapter 4 Results and Discussion		51
4.1	General Statements of Results	51

4.1.1	Idealised Skirt vs Deformed Skirt	51
4.1.2	Cushion Height vs Skirt Pressure	52
4.2	Pi Group Relationships	59
4.2.1	Pi Group 1-2 relationship	59
4.2.2	Pi Group 1-3 Relationship	61
4.2.3	Pi Group 1-4 Relationship	62
4.3	Optimum Configuration	63
4.4	Optimised Hover Height	65
4.5	Previous Studies	66
4.6	Expected Results	67
Chapter 5 Further Work		68
5.1	Prototype Testing	68
5.1.1	Construction	68
5.1.2	Testing	69
5.1.3	Validation of CFD model	70
5.2	Skirt Design	70
5.3	Net Torque Concerns	71
5.3.1	Principle of Net Torque Rotation	71
5.3.2	Overcoming Net Torque	71
5.4	Blower Improvements	72

Chapter 6 Conclusions	74
6.1 Project objective 1	74
6.2 Project objective 2	75
6.3 Project objective 3	76
6.4 Project objective 4	77
6.5 Summary	77
References	79
Appendix A Project Specification	83
Appendix B Pi Group Models	84
Appendix C Board Dimensions	85
Appendix D FEA Reports	86
Appendix E Risk Assessment	94

List of Figures

Figure 1-1 Airflow through system.....	3
Figure 2-1 Typical Ionocraft Arrangement (Ianculescu, Sohar & Mudrik, 2011)	11
Figure 2-2 Internal Workings of Maglev Train (Shanghai Maglev Transportation Development Co., 2005)	13
Figure 2-3 Standard Hovercraft Components from (Harrison, 2004)	14
Figure 2-4 Air-Gliding Skateboard (Shan et al., 2008)	18
Figure 3-1 Board Lift Area.....	23
Figure 3-2 Ozito OZBL 1800WA 240V Electric Leaf Blower	24
Figure 3-3 Leaf Blower validation schematic	25
Figure 3-4 Leaf Blower Test Setup	26
Figure 3-5 Leaf Blower Test - Flow Meter, Pressure Sensor and Ball Valve.....	27
Figure 3-6 Leaf Blower Test Results.....	30
Figure 3-7 Outlet Air Velocity for specified Air cushion Heights	34

Figure 3-8 Dimensionless Pi Groups	37
Figure 3-9 Skirt profiles.....	39
Figure 3-10 Preliminary Mesh.....	40
Figure 3-11 Side view of preliminary mesh	41
Figure 3-12 CFD Simulation Domains.....	43
Figure 3-13 CFD Simulation Domains.....	44
Figure 3-14 CFD Simulation Domains.....	45
Figure 3-15 Sample of Steady State conditions for monitored values.....	48
Figure 4-1 Sample Histogram plot of pressure over "Average Skirt Pressure" domain.....	52
Figure 4-2 Plot of Skirt pressure for varying air cushion heights in preliminary simulation configuration.....	53
Figure 4-3 Top View of Pressure Distribution Plot on Inlet, Average Skirt Pressure and Ground Domains for $h=0.5\text{mm}$ preliminary simulation.....	55
Figure 4-4 Underside view of Pressure Distribution Plot on Ground, Average Skirt Pressure and Inlet domains for $h=0.5\text{mm}$ preliminary simulation.....	55
Figure 4-5 Side View of Velocity Streamlines for $h=0.5\text{mm}$ preliminary simulation	56
Figure 4-6 End View of velocity streamlines for $h=0.5\text{mm}$ preliminary simulation INSET - Velocity streamlines through air cushion	57

Figure 4-7 Isometric View of velocity streamlines for $h=0.5\text{mm}$ preliminary simulation.....	58
Figure 4-8 Relationship between Pi Groups 1 & 2 for three values of N	59
Figure 4-9 Relationship between Pi Groups 1 & 3 for three values of N	61
Figure 4-10 Relationship between Pi Groups 1 & 4 for three values of N	63
Figure 4-11 Optimised configuration Skirt Pressure for varying skirt heights....	65
Figure 5-1 Possible Experimental Testing Setup	69

List of Tables

Table 3-1 Leaf Blower Test Results (All pressures are gauge)	28
Table 3-2 Test Range for CFD and Dimensional Analysis	32
Table 3-3 Boundary Conditions for Fluid Simulation.....	46
Table 4-1 Optimum Skirt Configurations	64
Table 6-1 Optimum values for specified parameters.....	75
Table B-1 Parameters for Simulation Models	84

Nomenclature and Acronyms

<i>CAD</i>	Computer Aided Drafting
Li-Po	Lithium Polymer
NiMH	Nickel-metal Hydride
ACV	Air Cushion Vehicle
<i>CFX</i>	Fluid Dynamics Simulation Software
ANSYS	Fluid Dynamics Simulation Software

Chapter 1

Introduction

1.1 Background

A Skateboard is a type of sporting or recreational equipment made of Maplewood board approximately 16 mm thick and has two sets of wheels on which it rolls. The skateboard is generally propelled forward with one foot while the other remains on the board, or alternatively it can be used in skate parks and half pipes. Since the release of the 1985 movie "Back to the Future" people worldwide have entertained the idea of a "hoverboard", a device similar to a skateboard but one that hovers above the ground. This project aims to move toward the eventual development of a marketable and effective hoverboard using the concept of an air bearing to keep the rider elevated from the ground.

1.2 Outline of the Study

The outline of this study is to expand on the research conducted by (Shan, 2008) in the development of a marketable hoverboard. A review of available technologies will highlight that an air cushion is currently the most practical method of keeping

the board elevated from the ground using a battery power source. Through the optimisation of the outlet air holes the mechanical efficiency of the system can be improved and therefore reduce the power requirements. This will improve the flight time and marketability of the hoverboard.

1.3 Problem Outline

This project aims to improve the design of the novel air-gliding (hovering) "skateboard" proposed by Shan et al. (2008) by optimising hole location, hole diameter, number of holes and inlet velocity. The results presented in the paper by Shan et al. (2008) predict a co-efficient of static friction between the base of the board and the ground of 0.0088 and a co-efficient of kinetic friction of 0.0034. Further experiments determined that the optimum number of air outlet holes in the board was 44, as this reduced the standard deviation of the air outlet velocity to 3.7. The only parameters explored in the study by Shan et al. (2008) were the inlet velocity and the number of holes. The results published were valid for the dimensions of the board listed in the paper using a conventional air blower. The term *conventional* has been used due to the fact that detailed pressure, velocity, flow rate and power values for the experiment were not provided in the paper.

Through dimensional analysis and CFD modelling an optimum configuration of the above variables will be found. This will achieve a skirt design with consistent and stable outlet air velocities with minimum pressure losses. Minimising the pressure loss is critical to the future design of a self-contained Hoverboard as it will extend flight time by reducing power consumption.

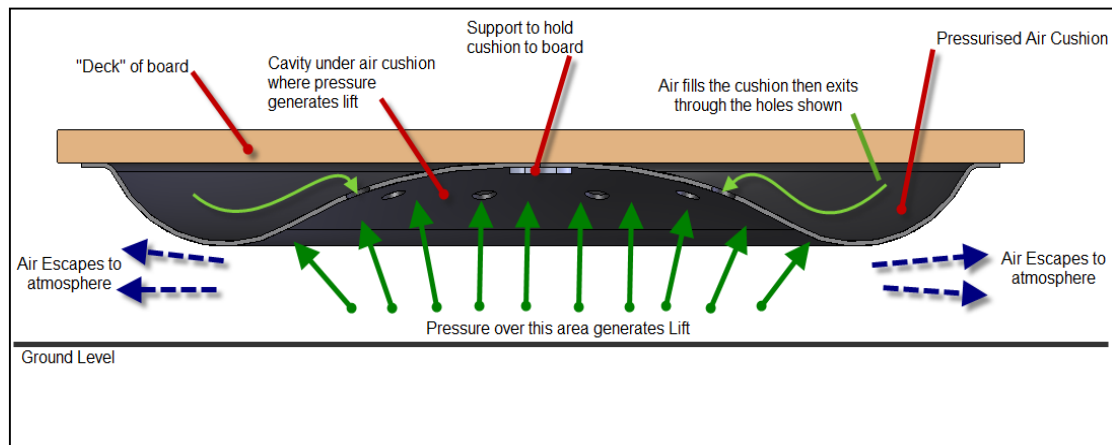


Figure 1-1 Airflow through system

An overview of the system and the airflow through the skirt is given in Figure 1-1. A prototype has been designed using the Solidworks CAD package and this model has been used for the CFD analyses carried out.

1.4 Research Objectives

The original project specification was to use CFD to validate the experimental results by Shan et al. (2008). Since then it has been decided that there is insufficient information provided by Shan et al. (2008) in relation to the control measures used for their experiments and the power source specifications. To overcome this, the power supply and geometry configuration data needed to be sourced by an alternate method. The most effective method of sourcing this data was through objectives 3 and 4 (below) which were defined in the preliminary project specification as tasks to be completed only if time permitted. A copy of the original project specification can be found in Appendix A.

This project has been broken down into four primary objectives. The first two of these primary objectives are essential points which form the basis of this

dissertation. The remaining two points were to be completed as time permitted. The objectives are listed here:

1. Use Computational Fluid Dynamic (CFD) simulations to validate the results of experiments conducted by Shan et al. (2008). The purpose of this objective is to compare numerical CFD results with the experimental results conducted by Shan et al. (2008), and discuss any discrepancies.
2. Use CFD and Dimensionless Analysis to optimise the cushion outlet hole design for minimum energy losses by analysing pressure and velocity variations in different geometry. This objective will expand upon the research already done by Shan et al. (2008) and propose an optimum hole configuration for a specified pressure and air velocity value. The factors to be optimised are the number of holes, hole diameter, hole location and inlet velocity.
3. Create a performance graph of the power source that is used for experimental testing. This is done experimentally to establish known values of static head, air velocity and power requirements for various volumetric flow rates of an Ozito OZBL 1800WA Leaf Blower. These values are then mapped on a performance graph so that optimum values can be selected. This optimum value is used in the CFD analysis and also in the experimental testing, to maintain consistency between the two.
4. Build and test a prototype model using the validated power source. This objective aims to use experimental results in a controlled environment to either validate or disprove the CFD results. The Ozito OZBL 1800WA Leaf Blower will be used in the experimental testing and will have the same pressure and velocity inputs that were used in the CFD modelling.

1.5 Methodology Summary

A literature review was undertaken to determine the status of Computational Fluid Dynamics modelling to optimise pressure requirements in a novel air-gliding skateboard. From this review it was found that only minimal research into this area has been done with the exception of the paper published by Shan et al. (2008) who proposed that a configuration of 44 outlet holes would minimise the standard deviation of the air outlet velocity. A review of this paper determined that there was insufficient data provided to accurately re-create the results. To overcome this issue arbitrary values were assigned to key geometry dimensions such as board length, width and skirt profile. To compliment these arbitrary values, experimental data regarding Leaf Blower performance was obtained to be used as an input in the Computational Fluid Dynamics model.

The parameters that would affect the fluid simulation results were then reduced to 4 Dimensionless Pi Groups using Buckingham's Pi Theorem. These parameters formed the basis for 21 different geometric models which were simulated in the CFD model and the results were plotted to show relationships between the key parameters.

These results were then interpreted and an optimum configuration for reducing pressure losses was selected. Validation of these results through experimental testing was not conducted in this study due to time constraints however the methods to be employed in this validation process have been covered in Chapter 5.

1.6 Project Contributions

The contribution of this project to the literature is the development of a simple Computational Fluid Dynamic model which predicts pressure drop through a given skirt design based on 4 key parameters. Minimising this pressure drop will be key to reducing power requirements for future iterations of an air-powered hoverboard concept. This concept also has the potential to be utilised in the research of other technologies, such as industrial devices which use air bearings as a medium to help transport heavy loads.

1.7 Consequential Effects

As this is a concept design only, there will be negligible impact on the community and environment as a result of construction and testing. What must be considered however, is the eventual effect of this product if it was to go into mass production. This process would have the potential to significantly impact the community and the environment both directly and indirectly. By assessing the points described by Green (2012), the magnitude of the consequential effects can be determined.

Over the life cycle of a Hoverboard, there would be some adverse environmental impacts due to the life cycle of Lithium Polymer batteries. For some time there was no recycling process available for Li-Po and NiMH batteries, however in 2011 Umicore (2014) created a factory designed expressly for the recycling of end of life rechargeable Li-Po and NiMH batteries. The potential of this technology reduces the adverse effects of the Hoverboard over its life cycle.

During the material acquisition phase of the manufacturing process renewable resources should be sourced. In general use of the hoverboard recycled timber would provide sufficient strength and this would further enhance the sustainability of the product.

Alternative methods for re-charging the Li-Po batteries should be researched. While this is beyond the scope of this project, Solar Power could be a viable option for recharging the batteries. If the top of the deck had solar panels integrated they would not only extend flight time but also potentially reduce recharge time and minimise environmental impacts.

There would be some potential risk to recreational users of this device. The risk associated with riding the board is comparable to that of riding a bicycle or skateboard. While all efforts will be made to make the riding experience as user friendly as possible, some risk must be assumed by the user. Given that skateboarding is such a popular sport, with little community backlash regarding injuries sustained while skateboarding, it has been decided that the assumed risk is acceptable. Any individuals using the Hoverboard would have a responsibility to read a user manual that would describe the safe operation of a board, and to ensure that they wore all recommended protective equipment.

In the event that this product was to be mass produced further research would be required on most of these topics however it is envisioned that there would be minimal adverse consequential effects. The controls mentioned above would limit environmental impacts as well as the risk to the community.

1.8 Dissertation Outline

An overview of each chapter in this dissertation is provided below.

1.8.1 Chapter 2 – Literature Review

This chapter provides a comprehensive literature review on different technologies that are available to generate lift in a hoverboard situation. Hovercraft are examined in detail as these are the most widely researched and similar product that could be found. The paper presented by Shan et. al (2008) is critically reviewed and its applicability to this study is assessed.

1.8.2 Chapter 3 – Methodology

This chapter presents the methodology used to determine accurate velocity and pressure data from an electric leaf blower. This data was then used as input for CFD models. The parameters of the CFD study were defined and justified. These CFD models were then combined with Dimensionless Analysis to determine the optimum skirt design for reducing the pressure drop between the inlet and the cavity underneath the skirt.

1.8.3 Chapter 4 – Results and Discussion

This chapter presents the results of the CFD simulations. It discusses the effects of the air gap on skirt pressure and specifies a maximum air gap allowable to still generate sufficient lift. The results for each CFD simulation are plotted to give relationships between the dimensionless Pi Groups so that an optimum configuration can be determined. This optimum configuration is then given and

the simulations to specify the maximum allowable air gap are re-run and the results compared to the initial simulation.

1.8.4 Chapter 5 – Further Work

This chapter presents a detailed look at the experimental testing procedure required to validate the numerical simulation. Other issues that have not been explored under the scope of this project are covered briefly and possible future improvements suggested.

1.8.5 Chapter 6 – Conclusions

This chapter summarises the results achieved and compares these to the original project specifications. The strengths and weaknesses of assumptions and results are discussed along with future improvements to the study.

1.9 Summary

Chapter 1 has provided a brief overview of this dissertation and the methods used to solve the project objectives. A brief introduction into each of the remaining chapters has also been included. It should also be noted at this point that all images and photographs in this document have been created by the author except where otherwise acknowledged.

Chapter 2

Literature Review

A review of current technologies capable of providing lift will be conducted to highlight that an air cushion is currently the most practical method for a hoverboard application. Current hovercraft systems will be reviewed in detail and also techniques used for dimensional analysis and optimisation.

2.1 Ionocraft

An Ionocraft, pictured in Figure 2-1 on page 11, is a small craft that generates lift through the Biefeld-Brown Effect (Chen, Rong-de, Bang-jiao 2013). The Biefeld-Brown Effect was developed by physicists Thomas Brown and Dr Paul Biefeld (Mallove, 2002) and is the application of high voltage electricity to an asymmetric capacitor, which produces lift.

To produce the lift the Ionocraft is electrically charged which ionises the air around it. The top of the craft is covered with positive electrodes, while the bottom of the craft is covered in negative electrodes. It is important that these electrodes have sharp edges to allow easier ionisation of the air (Chen, Rong-de, Bang-jiao

2013). Mallove (2002) states that as the air encounters these positively charged electrodes at the top of the craft, the molecules in the nearby air are torn off which creates a cloud of positively charged ions. These positively charged ions are then drawn towards the negatively charged ions at the bottom of the craft, which creates a vacuum at the top of the craft and denser air at the bottom resulting in lift.

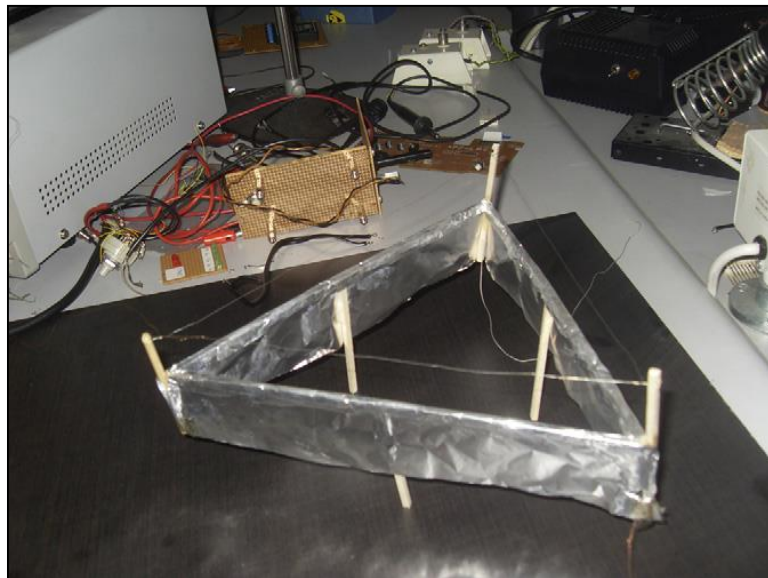


Figure 2-1 Typical Ionocraft Arrangement (Iancu, Sohar & Mudrik, 2011)

While the effect has been confirmed to exist, the theory behind what causes the lift still remains to be satisfactorily explained (Chen, Rong-de, Bang-jiao 2013). It is proposed by (Chen, Rong-de, Bang-jiao 2013) that the Biefeld-Brown Effect relies on one of three theories; Theory of Ion Wind also known as Electrohydrodynamic thrust, Theory of Ion Drift or the theory of Lift in a vacuum and zero-point energy explanation.

Of these three theories it seems likely that each is responsible for some percentage of the lift generated. A review of these three theories by (Chen, Rong-de, Bang-jiao 2013) shows that scientists have succeeded in proving that each theory

accounts for only a percentage of the actual lift produced in experiments. Of the three theories (Chen, Rong-de, Bang-jiao 2013) propose that Ion Drift is generally accepted to be the most accurate explanation of the Bifeld-Brown effect. Work conducted by (Ianculescu, Sohar & Mudrik, 2011) counters this point and suggest that it is the theory of Ion Wind that generates the largest percentage of lift. From this it can be deduced that while each theory is valid, the full source of lift is yet to be fully understood. Further research in this area is required before a definitive theory can be produced. As a method of lift for an Air-Gliding Skateboard, the Ionocraft is not suitable due to battery power restrictions. At the current level of research in the area Masuyama & Barrett (2014) give the thrust to power ratio as $100 \text{ N}\cdot\text{kW}^{-1}$. This means that for a 100 kg total weight of board and rider, there would be a requirement for 10kW of power. One of the project aims is for this design to eventually be marketable and battery operated, which is not possible with the power requirements of an Ionocraft.

2.2 Magnetic Levitation

Magnetic Levitation has evolved recently as an effective method of reducing friction between surfaces. The ability to suspend an item using only magnetic force reduces contact between moving and stationary parts, which eliminates friction (Kumar & Jerome, 2013). Most notably has been the development of the Maglev train system in China. The concept of the Maglev train originated in Germany as early as 1922 (SMT, 2005) with the work of Hermann Kemper. This work continued until the first successful commercial Maglev train line was installed in China in December 2002.

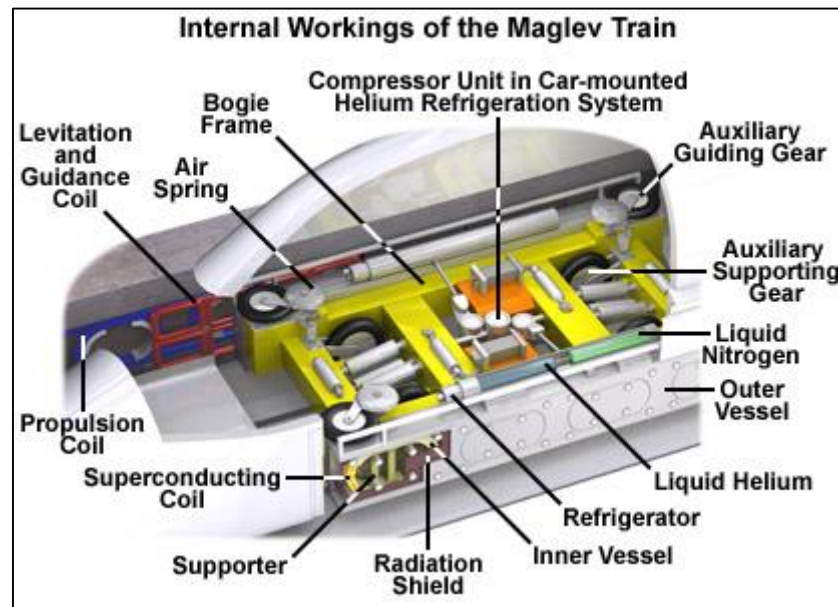


Figure 2-2 Internal Workings of Maglev Train (Shanghai Maglev Transportation Development Co., 2005)

Radboud University (2014) explains that magnetic levitation is when two magnetic materials are either attracted to each other or repelled by each other with a force dependent on the magnetic field and the area of the magnets. This principle is shown in Figure 2-2. One of the key problems with Magnetic Levitation is the stability of the magnets. If Dipole magnets are placed on top of each other with like poles facing together, then the magnets will “slide” off to the side. To overcome the stability issues Schmidt proposes the use of Cu/CuNi/NbTi mixed matrix conductors and reports that a stability model depending on the transient heat transfer was obtained.

The downside of Magnetic Levitation in respect to the Hoverboard concept, is that Magnetic Levitation requires a lot of infrastructure. To use Magnetic Levitation a track or area would need to be designed as a platform for the magnetic levitation. This contradicts the project aims of providing a marketable recreation product. It is for this reason that Magnetic Levitation technology has not been pursued any further for the scope of this project.

2.3 Air Operated

2.3.1 Hovercraft

The hovercraft concept can be traced back as early 1716 and Emmanuel Swedenborg, however Amyot (1989, p. 1) credits the practical form that is seen today to have originated with Christopher Cockerell's annular jet principle published in 1955. Airlift Hovercraft (2013) define a Hovercraft or ACV (Air Cushioned Vehicle) as a machine that operates by "producing a cushion of air between the craft's hull and the surface below". Further characteristics include the ability to operate over virtually any flat surface such as ice, flood plains, vegetation, sand, gravel, mud flats and shallow water.

While all hovercraft vary depending on their specific requirements, they also share some key components. Figure 2-3 shows a simplified hovercraft with key components numbered.

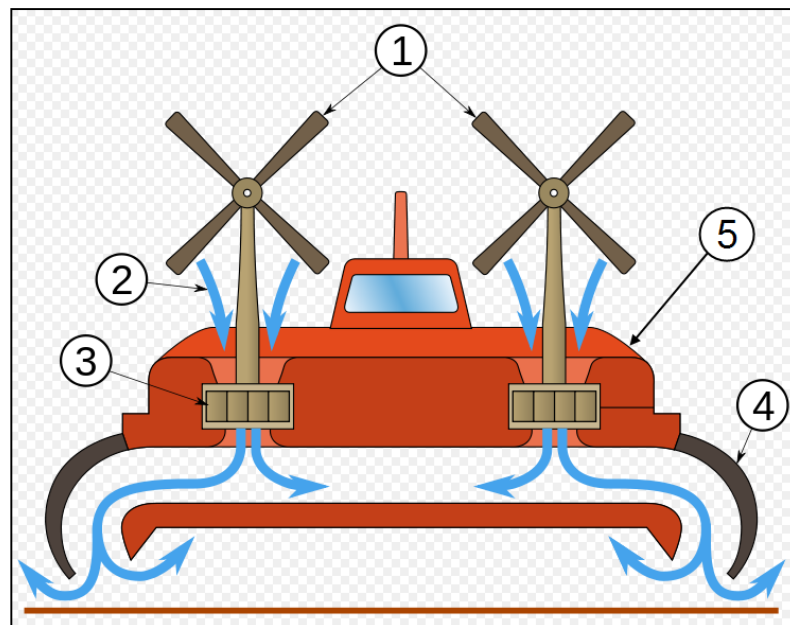


Figure 2-3 Standard Hovercraft Components from (Harrison, 2004)

Item 1 shows the propulsion fans at the back of the craft. These generate forward and backward thrust and allow for braking and steering. Air (item 2) from the atmosphere is drawn in by centrifugal blowers (item 3) and a pressure rise is generated under the Hull (item 5). As the pressure increases the flexible skirt (item 4) is inflated, and eventually the excess air escapes underneath this skirt.

The mechanical resistance of the craft is reduced by the fact that it rides on a cushion of air, which eliminates rolling resistance. This means that to generate forward motion the craft only needs to overcome air resistance and friction between the air cushion and the ground. The downside of this design is that the craft must generate enough lift to remain elevated from the ground, in contrast to vehicles that operate on a wheeled system. Amryot (1989, pp. 6) states that due to inherently low frictional resistance between the air cushion and the ground, hovercraft can maintain efficient operation at a range of speeds between 15.4 and 41.15 m/s.

The skirt is one area of the hovercraft which must be carefully considered in the design phase. There are several aspects of hovercraft flight which are directly impacted upon by skirt design. Amryot (1989, pp. 7) lists the function of the skirt as:

- The means of containing the air cushion beneath the hull to raise the craft above obstacles.
- A main contributor in the stiffness and damping of the air cushion beneath the hull, in this sense the skirt is the suspension system.
- Contributing to stability and manoeuvrability of the craft

Chung and Jung (2003) used genetic algorithms to optimise the heave vibration through skirt design on two models of hovercraft; CCG's Waban-Aki and the US Navy's LCAC. In their findings they concluded that heave vibration was able to

be significantly reduced through skirt optimisation, and thus reaffirmed Amryot (1989) that skirt design is critical in a dynamic hovercraft system.

In the air cushion the power source is the centrifugal blowers, which are used in the lift fan system to generate pressurised air at a cushion pressure and cushion flow. To generate sufficient lift for Craft Weight W (N), Amryot (1989, pp. 48) proposes that W must be equal to or exceeded by the cushion pressure P_c (Pa) acting over the planform area of the craft A_p (m^2):

$$W = P_c \times A_p$$

And also that Lift Power P_{Lift} (W) is a function of airflow Q (m^3/s) and cushion pressure;

$$P_{Lift} = Q \times P_c$$

It is then further proposed by Amryot (1989, pp. 49-52) that the lift power is often only 1/3 of the total on-board power. Additional mechanisms are used to stabilise ride control such as puff ports, bow thrusters and vents which assist with turning and banking in any direction.

In conclusion Amryot (1989, pp. 52-54) concludes that the height h at which the craft hovers above the ground is a function of volumetric flow rate Q , the outlet velocity V_e , and the planform area A_p of the craft. The equation for flow rate as a function of A_p and V_e is given by Amryot as:

$$Q = A_p \times V_e$$

Where A_p is a function of craft length L (m), width B (m), and height h (m) from the ground:

$$A_p = 2(L + B) \times h$$

These simplified equations that were used by Amryot (1989) will be used in the initial consideration of this project. Additional factors such as velocity and pressure losses in the system will be incorporated into the system analysis.

There have been many variants of the hovercraft system designed and sold since its creation in 1955. The uses range from the novel Airboard that was used in the Sydney Olympics opening ceremony, to recreational private use hovercraft and large scale military applications for beach landings. Regardless of the application each of these designs uses the same basic principles outlined in this section.

2.3.2 Air-Gliding Skateboards

To date very little work has been done on adapting current hovercraft technologies to a smaller scale for use in a hoverboard. This concept was explored by Shan et al (2008) and proven to be a viable method of lifting a payload of approximately 60 kg. Shan et al. (2008) propose that the hole configuration in the cushion design plays the most important part in a hoverboard concept, thus confirming Chung and Jung (2003) and Amryot (2009) that skirt design is a critical factor for a hovering system. Through fluid modelling two variables were optimised. These were the outlet hole locations and the number of outlet holes. Minimum pressure loss was the key factor to be optimised along with minimum standard deviation in outlet hole velocity. It was then reported by Shan et al. (2008) that for inlet air velocity of 120 mph (53.65 m/s) the optimum configuration was 44 holes located 0.06 m from the board centreline, for a board length of 1.15 m and width 0.065 m. From the report it can be seen that this optimum configuration is only valid for the inlet velocity and outlet hole diameter listed in the report. It is assumed, based on Amyrots (1989) assertion that outlet velocity V_e directly affects the hover height h above the ground and that varying the inlet velocity and outlet hole

diameter would greatly affect the optimum configuration. An overview of the skirt design presented by Shan et al. (2008) is given in Figure 2-4 below.

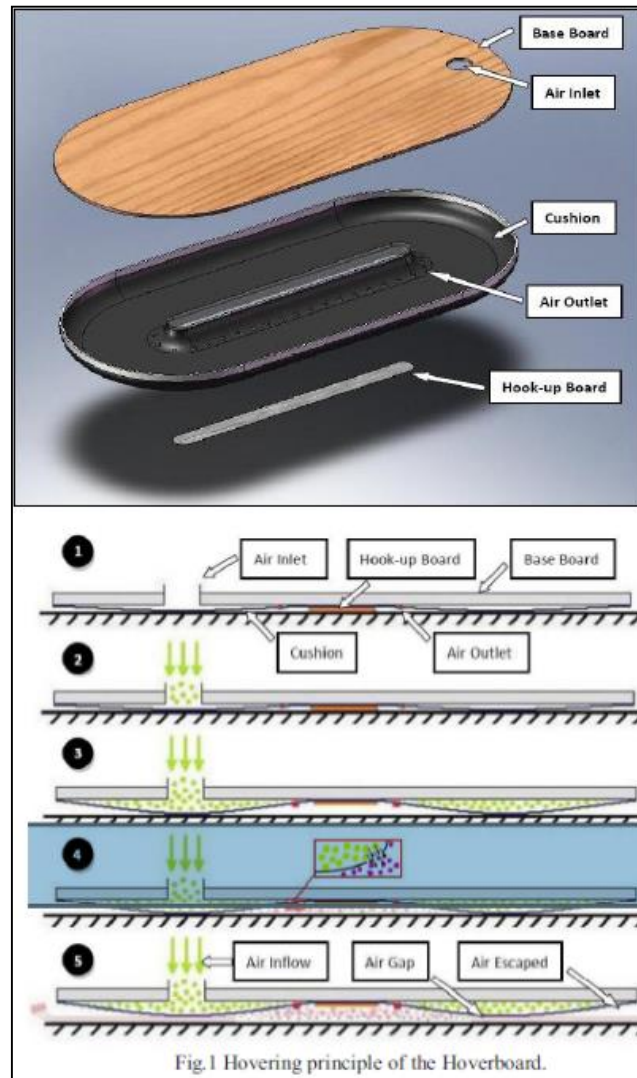


Figure 2-4 Air-Gliding Skateboard (Shan et al., 2008)

This leads to the conclusion that further work in this area is required before the most efficient system is determined. It is also noted that the experimental setup shown in Figure 2-4 has an air inlet at one end of the board only. It is highly likely that this would drastically affect the deviation in outlet hole velocities and pressures due to the non-symmetrical nature of the design. Inlet holes at both ends are expected to provide a much more even flow along the majority of the holes.

To compensate for this a design with two inlet sections will be considered for the purpose of this project.

2.4 Dimensional Analysis

Most phenomena in fluid flow depends on a complex array of geometry and flow parameters. Dimensional Analysis is defined by Pritchard (2011, pp. 294 – 296) as a process of reducing these parameters down to form a single relationship or expression which defines the flow. The purpose of this form of analysis is to isolate key relationships between these parameters, the changing of which can offer significant insights into the nature of the flow phenomena. Sleight & Noakes (2008) highlight the significance of Dimensional Analysis in simplifying complex mathematical equations when dealing with fluid flow.

When obtaining data for a large number of parameters Dimensional Analysis can significantly reduce the number of experiments required. Pritchard (2011, pp. 294 – 296) states that for calculating the effects of drag on a sphere, the number of experiments could quickly reach 10^4 to accurately define the behaviour. This is time consuming and impractical. Sleight & Noakes (2008) reinforce this belief and state that not only does Dimensional Analysis reduce the number of experiments, it provides insight into which measurements or parameters are the most important.

The most commonly accepted process of conducting Dimensional Analysis is defined by both Pritchard and Sleight & Noakes as the Buckingham Pi Theorem. This process is a clearly defined method of obtaining the correct parameters and their dimensionless relationships. In order to obtain the dimensionless relationships, the Buckingham Pi Theorem requires each parameter to be reduced

to primary units of Mass (M), Length (L) and Time (t) or Force (F), Length (L) and Time (t). These primary units are not exclusive, and if other units such as quantity are required then they may also be included.

Examples of Dimensional Analysis that are used commonly are listed by Pritchard (2011, pp 296-298) as the Reynolds Number, Prandtl Number, Euler Number, Froude Number, Weber Number and Mach Number. These are just some examples of the benefits of Dimensional Analysis.

Chapter 3

Methodology

Chapter 3 presents the methodology used in this study to an assessment of the minimum power requirements for a hoverboard of specified dimensions to ensure the feasibility of the project when using commercially available products in the design. Part of this requirement is to determine the optimum skirt design for reducing pressure losses in the system. CFD is the method of choice for this study as it eliminates the requirement of multiple prototype constructions that would be required for experimental testing. A CFD model allows the design to be refined multiple times quickly and at low cost. Experimental validation of the CFD model will be required to confirm its validity however this is beyond the scope of this report. This Chapter will then cover how data was collected for the CFD simulation, how that data was input into ANSYS 15.0 CFX, what conditions were used for the simulation and finally provides comments on the validity of CFD model. It also covers the dimensional analysis techniques used to reduce the number of simulations required.

3.1 Key Design Constraints

This section will highlight the critical design parameters for an electric powered hoverboard. An assessment of the minimum power requirements and the available power sources was carried out to ensure that the goal of a working hoverboard is achievable. Section 3.1 outlines the experimental methods that were used to obtain the data required for the CFD simulation and comments on the validity of these experiments.

3.1.1 Minimum Pressure Requirement

One of the key parameters of this project is that it must contribute towards the development of a marketable hoverboard. As part of this endeavour a brief overview of the system as a whole is to be considered. This overview aims to highlight any foreseeable issues with power technologies and blower performance, the design of which are beyond the scope of this project.

Due to the fiscal restraints inherent with this research project, it has been asserted that any materials required be current, commercially available products that can be utilised with only minor modifications. In keeping with the experiments conducted by Shan et. al (2008), a domestic 240V leaf blower will be used as the power source. Before moving to a production phase for this project additional research is required to optimise the power and blower system, which is beyond the scope of this project

In order to ensure that this project remains realistic in terms of marketability, it is imperative that the air delivery system can be battery operated and self-contained. An extensive literature review has concluded that at the time of this

project no other viable power option was available. To assess the power requirements, some preliminary calculations were performed to allow the comparison of available battery power and expected power requirements. Some variables have been arbitrarily assigned for the purpose of this study in the absence of any other data from past experiments. These are defined below and in Figure 3-1:

$$\text{Payload (Board + Rider)} = W = 100 \text{ kg} \approx 1000 \text{ N}$$

$$\text{Effective Cushion Width} = B = 0.225 \text{ m}$$

$$\text{Effective Cushion Length} = L = 0.510 \text{ m}$$

$$\text{Board Lift Area} = A_p = \pi \left(\frac{B}{2} \right)^2 + B \times L = 0.1545 \text{ m}^2 \quad (\text{Equation 3-1})$$

$$\text{Perimeter Board Lift Area} = L_{\text{Board}} = \pi B + 2L = 1.7269 \text{ m}$$

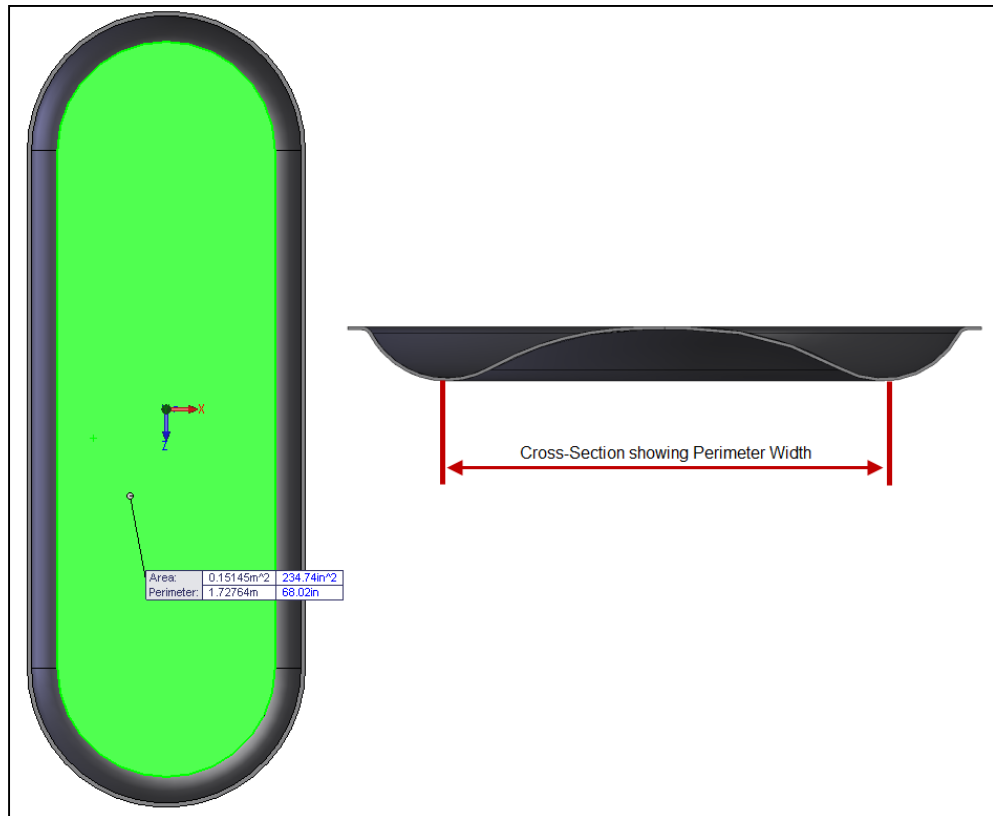


Figure 3-1 Board Lift Area

Figure 3-1 shows the Lift Area and Perimeter defined as the area under the skirt that will be reacted upon to provide a lift force. The perimeter of this area is the tangent point at which the air skirt is lowest.

To calculate the minimum required gauge pressure (P_{min}) the following equations were used:

$$P_{min}(Pa) = \frac{W}{A_{Board}} = \frac{1000}{0.1545} = 6472 Pa \quad \text{Equation 3-2}$$

Once the minimum pressure requirement was determined, a commercial blower was sourced to satisfy this requirement. A margin of around 8% was introduced to allow for unexpected system losses and the minimum pressure requirement was therefore specified as 7000 Pa.



Figure 3-2 Ozito OZBL 1800WA 240V Electric Leaf Blower

The blower used is shown in Figure 3-2. To solve the equations provided by Amryot (2009) in section 2.3.1, it was determined a volumetric flow value is required. While some manufacturer data was available on this item, a performance

graph listing volumetric flow rate against pressure was not available. In addition to this, the leaf blower used for the testing was not brand new and had been in service for approximately 2 years. To compensate for this, it was necessary to map the performance of the leaf blower to ensure that it was able to provide the minimum pressure requirement.

3.1.2 Validation of Commercial Leaf Blower

To validate the power source a setup was constructed as shown in Figure 3-3. As far as was practicable, steps were taken to reduce the impact of turbulent flow on the measuring devices.

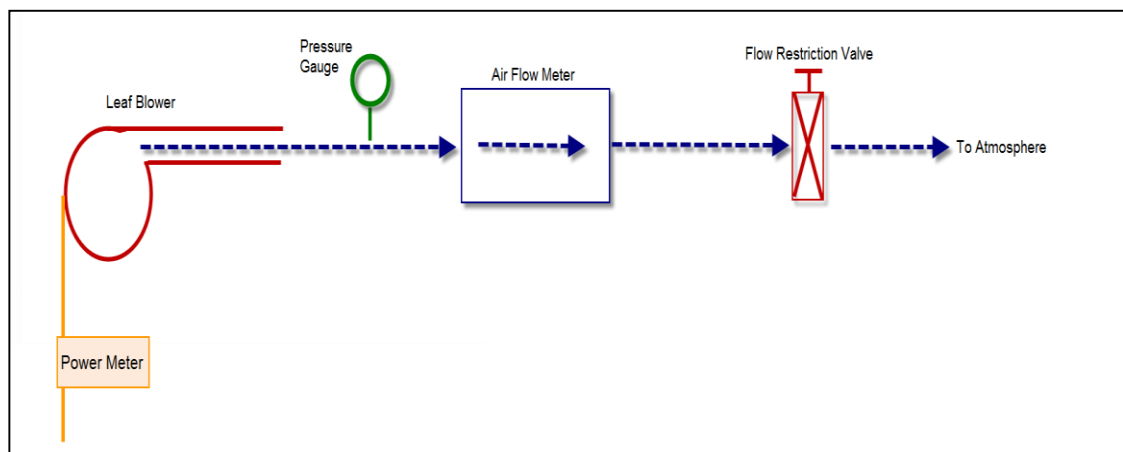


Figure 3-3 Leaf Blower validation schematic

The outlet from the Ozito Leaf blower was stepped down to 19mm internal diameter PVC pipe which was the same size as the inlet to the flow meter. This was to ensure a smooth transition from the blower diameter to the flow meter inlet which encouraged laminar flow and reduced turbulence. The PVC pipe was approximately 1m long, which allowed the flow to become fully developed when it reached the sensors.



Figure 3-4 Leaf Blower Test Setup

It is expected that some turbulence is likely to have been generated from the fittings used to connect the PVC pipe to the SMC flow meter, shown in Figure 3-4, however without customised testing apparatus this could not be avoided. All connections that were joined were tested for leaks by spraying a Water/Detergent mixture over the entire connection while the blower was operating. Any bubbles or signs of air leakage were then rectified to ensure accurate test data.

The validation setup for the leaf blower required accurate measuring equipment. From the earlier pressure calculations it was known that the minimum pressure required is approximately 6500 Pa (gauge). To ensure accuracy a Hydac HMG 3000 data recorder with low pressure gauge (0-9 Bar) was used to monitor the static gauge pressure. The Hydac Pressure Gauge recorded values to an accuracy of 1.0×10^{-4} Bar (10 Pa). A Power Meter provided by the University of Southern Queensland was used to record the real power and an SMC PF2A7 Digital Flow Switch was used to record the volumetric flow rate. All of these devices had current calibration labels ensuring the integrity of the experiment.

To control the air flow during the testing procedure, a JBS stainless steel Ball Valve was connected to the outlet of the SMC flow meter. These two devices were

used in conjunction to control the volumetric flow rate so that readings could be taken at 6 intervals.

The Hydac Pressure sensor was connected by a fitting that was drilled and tapped into the 1" BSP connection point of the PVC pipe. The fitting was screwed in until it was flush with the internal diameter of the PVC pipe to minimise its effect on the fluid flow. This sensor was positioned as close as possible to the SMC flow meter, as shown below in Figure 3-5, so that static pressure and flow readings would be taken for a similar region of the fluid.



Figure 3-5 Leaf Blower Test - Flow Meter, Pressure Sensor and Ball Valve

It is likely that there were some pressure and velocity losses introduced into this system by the nature of the testing procedure. These are the losses due surface friction forces in the boundary layer, kinetic energy losses as the air imparts kinetic energy to the pipes and energy losses due to heat conduction through the PVC pipe. As the Real Power was measured at the source, and the outlet velocity and pressure measured at the end of the system, it is reasoned that these losses are negligible in the design of a hoverboard system. While reducing these losses would

increase efficiency, it is not rated as a key parameter for this project, which instead is focused on the outlet hole design of the skirt. Once the optimum configuration of the board skirt has been achieved, these losses between the power source and the skirt can be assessed. It is far more practical to work on reducing these losses once the design of the air supply system from the blower to the skirt is finalised, which is beyond the scope of this project.

3.1.3 Leaf Blower Validation results

There were 6 intervals that were used to record a set of data points during testing. The independent variable was the Volumetric Flow Rate, as this was controlled through the use of the JBS Ball Valve to set the intervals for data measurement. Once the full range of the flow had been established, by operating the valve fully open and fully closed, this range was divided into smaller equal domains. The results are shown below in Table 3-1.

Static Pressure (kPa)	Dynamic Pressure (kPa)	Stagnation Pressure (kPa)	Flow (m ³ /s)	Flow (L/min)	Real Power (kW)
170.0	0.00000	170.00	0.00000	0.00	1.41
169.5	0.03547	169.54	0.00217	130.26	1.42
169.0	0.13578	169.14	0.00425	254.85	1.43
168.0	0.24139	168.24	0.00566	339.80	1.43
167.0	0.42913	167.43	0.00755	453.07	1.44
166.0	0.67051	166.67	0.00944	566.34	1.45
165.0	1.00619	166.01	0.01156	693.76	1.45

Table 3-1 Leaf Blower Test Results (All pressures are gauge)

The Dynamic pressure was calculated using Bernoulli's principle in the form given by Pritchard (pg 255):

$$P_{dynamic}(Pa) = \frac{1}{2}\rho V^2 \quad (\text{Equation 3-3})$$

It should be noted here that Bernoulli's equation is only valid for the following conditions:

1. Steady flow
2. No friction
3. Flow along a streamline
4. Incompressible flow

The experiment was conducted at ambient an ambient temperature of 22°C and all density values were assumed to be constant at 1.225 kg/m³. The velocity was calculated by using the volumetric flow rate and the internal pipe area at the inlet to the SMC flow meter. The pipe internal diameter was 19mm and the area was $2.835 \times 10^{-4} \text{ m}^2$.

$$V = Q/A$$

The stagnation pressure was calculated as the sum of the dynamic and static pressures.

The results obtained from this experiment showed trends that were consistent with other blower performance curves that are available for comparison. As the volumetric flow rate increased, the power requirement increased almost linearly. This relationship is caused by the fact that to generate additional volumetric flow, more energy is required which in turn increases the power requirement. The pressure decreased with increasing flow rate as expected.

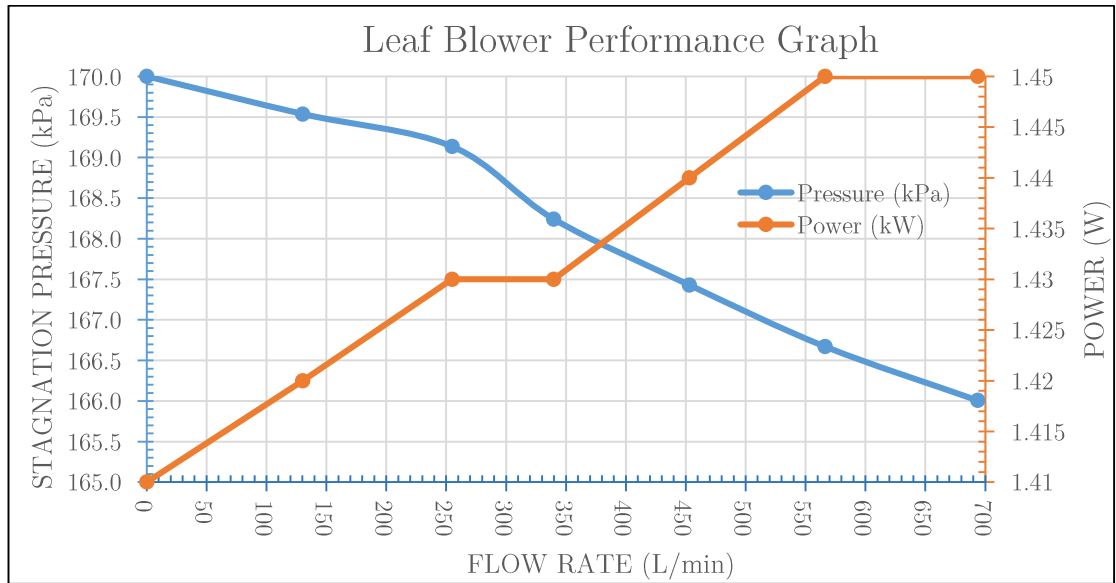


Figure 3-6 Leaf Blower Test Results

The data presented in Table 3-1 has been shown in Figure 3-6. Using this data and Equation 3-2 it can be determined that a conventional leaf blower will generate sufficient lift to carry a payload of 100 kg. The power requirement must then be balanced with the volumetric flow rate. A higher volumetric flow rate will increase the height of the air cushion which is the most desirable outcome. A higher air cushion will compensate for uneven surfaces over which it will operate. To counteract this point however, is that the higher flow rate requires more power, which will in turn reduce battery life. It has been reasoned that the gains in volumetric flow rate outweigh the negatives of additional power requirement. Therefore it is assumed that a leaf blower would operate at 100% capacity if it was used to power a hoverboard. This would mean that it would be operating at 1.45 kW, 0.01156 m³/s and producing a gauge pressure rise of 166.01 kPa.

Pritchard (2011, pg 242) states that the maximum acceptable Mach number for a fluid to be considered incompressible is 0.3. The maximum volumetric flow rate provided by the Ozito Leaf Blower was found to be 0.01156 m³/s. This value can

then be used in the equation given by Pritchard (2011, pg 242) to determine the Mach number of a flow.

$$M \equiv \frac{V}{c} \quad \text{Where} \quad \begin{array}{l} M = \text{mach number} \\ V = \text{flow speed} \\ c = \text{speed of sound for air at STP} \approx 343 \text{ m/s} \end{array}$$

This equates to a fluid velocity of approximately 103 m/s. To remain below this velocity (based on a volumetric flow rate of 0.01156 m³/s), the minimum area in the system at any point through which the fluid flows must be greater than 3.853×10^{-4} m². This simple check will ensure that the project does not enter the region of compressible flow. If however the geometry requirements create a situation where the flow may become compressible, the analysis used can be re-evaluated.

It should be noted at this point that if this product were to become marketable, some significant research into fan design would need to occur. The additional pressure generated by the leaf blower system is wasted energy. As the pressure increases above P_{min} the board will lift off the ground and increase the air gap h underneath it, thus reducing the pressure produced. Some pressure rise could be sacrificed for increases in volumetric flow rate and therefore reduce power requirements.

3.1.4 CFD Parameters

Once the “commercial” leaf blower performance had been experimentally determined, design constraints were created for the fluid simulation modelling. Based on the premise that the hoverboard is to be constructed from readily available products, the following range of values have been listed in Table 3-2.

Property	CFD Input Value from Figure 3-6	Experimental Test Range from Table 3-1	Range Simulated for CFD and Dimensional Analysis
Stagnation Gauge Pressure (kPa)	165	1.65 - 1.7	166.01
Power (kW)	1.45	1.41 - 1.45	N/A
Flow Rate (m ³ /s)	0.01156	0-0.011563	0.011563

Table 3-2 Test Range for CFD and Dimensional Analysis

The height of the board from the ground is expected to vary depending on the pressure underneath the skirt and the downward force generated by the weight of the rider W . As the pressure under the board builds, it will rise higher from the ground. As it rises higher from the ground however, the pressure underneath the board will begin to decrease as there are less friction effects from the boundary layer shear forces acting on the fluid that passes between the skirt and the ground. These boundary layer forces will resist the flow and therefore generate a pressure rise. In essence, it is expected that the board will oscillate slightly until it reaches an equilibrium point of steady state flow.

It should also be noted that in reality the effective area of the board A_p would vary slightly as the skirt deforms and moves the tangency point. The pressure near the tangency point between the skirt and the ground would also vary almost linearly thus further affecting skirt deformation. Skirt deformation would then be found through a complex set of dynamic equations relating pressure, pressure drop through the holes, skirt stiffness, skirt geometry and the pressure gradient near the tangency point between the skirt and the ground. To examine this phenomenon in detail is an extensive project in itself and likely unjustifiable in terms of the time consuming nature of this sort of analysis. If the precise dynamics of skirt deflection were required experimental testing on prototypes would almost certainly prove to be the most efficient method. A detailed analysis of this skirt

deformation is beyond the scope of this project as it is expected to negligibly impact the pressure drop between the inlet and the cavity under the skirt.

It has been assumed for the purpose of the simulation that steady state flow has already been reached. This will be simulated by modelling the air gap which produces only the minimum pressure rise required. The reasoning behind this is that any further pressure rise would simply cause the board to rise higher and when it did the pressure would begin to drop. As the pressure drops the board ride height would decrease, thus generating the oscillating motion. The inlet velocity has been calculated based on the value $Q_{in} = 0.01156$ from Table 3-2 and two 54 mm diameter inlets.

$$V_{in} = \frac{Q_{in}}{A_{in}} = \frac{0.01156}{0.004580} = 2.524 \text{ m/s}$$

For the purpose of the feasibility study, it has been assumed that there is no loss in the volumetric flow rate through the system. This leads to the equations

$$Q_{in} = Q_{out}$$

$$V_{out} = \frac{Q_{out}}{A_{out}} = \frac{Q_{out}}{L_{Board} \times h}$$

From these calculations the expected velocity to board height dimensions have been plotted in Figure 3-7 Outlet Air Velocity for specified Air cushion Heights on page 34. It is therefore expected that a hoverboard constructed to the dimensions shown in 3.1.1 would lift a payload of 100kg with an air cushion of 0.65 mm – 3mm with a power requirement of 1.45kW. Given that the output pressure of the blower at 0.01156 m³/s is 166.01 kPa, it has been reasoned that a pressure rise of 7 kPa is easily achievable. The reasoning behind this is that if there was to be an air gap of 0mm, then the blower would essentially create a

pressure of 166 kPa throughout the entire system. As this is high enough to lift the board, it is reasoned that once 7 kPa has been reached the board will lift off the ground.

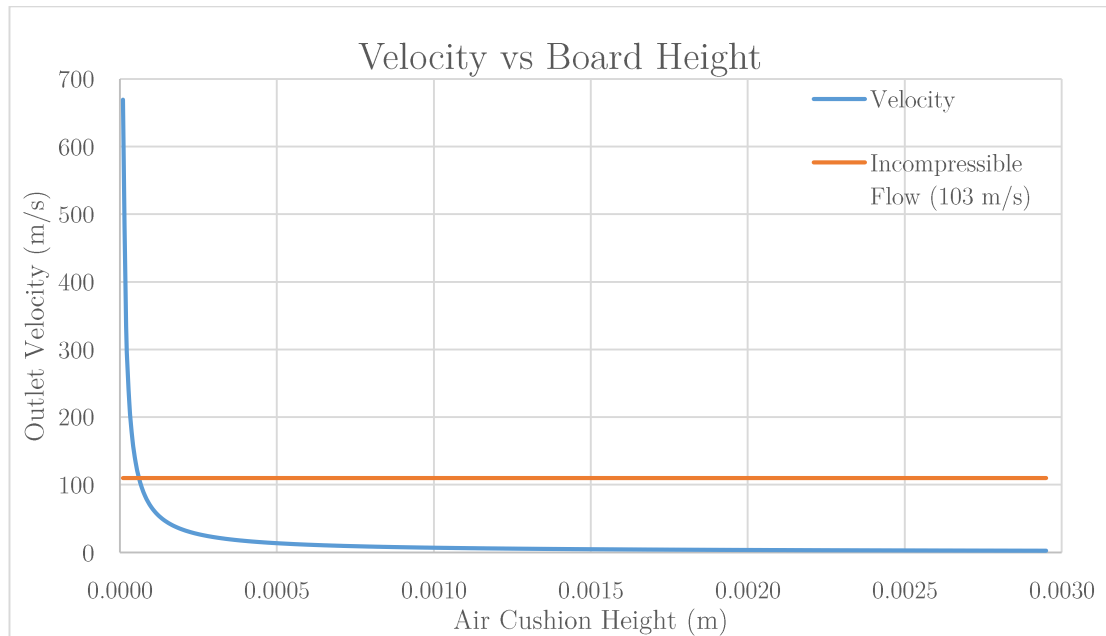


Figure 3-7 Outlet Air Velocity for specified Air cushion Heights

Given these values the following components were sourced from HobbyKing (2014):

- Turnigy RotoMax 1.60 Brushless Outrunner Motor: 10 Cell 37 V Battery, RPM:231 kv, 2960W, 80 A.
- Turnigy K-Force Speed Controller: Continuous 120 A Output, 5-12 Cell Input
- 4 x ZIPPY Compact 5800 mAh 10 S 25 C Li-Po Battery Pack; 5800 mAh capacity, 10 Cell at 37 V, 25 C Continuous Dishcharge.

These components provide enough power to operate an Ozito blower at 100% system power for around 15 minutes of ride time. The total weight of this setup comes to approximately 15kg, which reduces the maximum rider weight to 85kg. As a feasibility study this data is considered accurate enough to justify further investigation into the optimisation of the design. In the event that this product

moves to a marketable stage, further research into blowers and power sources will be required.

3.1.5 Summary

The results from the experimental testing of the Ozito OZBL 1800WA 240V Electriv Leaf Blower have been included in the methodology as they form a critical part of the CFD analysis. From the results of the performance test on the Electric Leaf Blower it has been concluded that a battery operated hoverboard system could be constructed using commercially available products. For the purpose of the CFD simulations and dimensional analysis a range of realistic values has been listed in Table 3-2. This range has been extended from the results gained in the experimental testing of the leaf blower performance to include possible configurations that could be achieved with further blower refinement studies.

3.2 Dimensional Analysis

Section 3.2 covers the process of Dimensional Analysis which was used to reduce the number of simulations required. There were assumed to be 5 variables, listed in Section 3.2.2, which affect the pressure drop (ΔP) throughout the system. A minimum of three different values are required for each independent variable in order to establish a trend. If each of the independent variables was calculated 3 times against each possible value for the remaining variables, this would lead to 6^3 (216) simulations required in order to select an optimum configuration. In order to reduce this number of simulations, Buckingham's Pi Theorem has been used to create non-Dimensional parameters. By creating these non-dimensional parameters, the total number of simulations required has been reduced to 21.

3.2.1 Buckingham Pi Theorem

Five variables were optimised to find the configuration which reduced pressure losses in this system. These variables were inlet velocity, inlet pressure, number of outlet holes, outlet hole diameter and the distance between outlet holes and board centreline. If 5 increments for each variable are selected, then there is a total of 3125 (5^5) potential combinations. Due to the time consuming nature of running a fluid simulation, running each of these simulations would be impractical and it is unlikely that they could be completed within the proposed timeline.

Shehadeh et al (2014) propose that Buckingham's Pi Theorem is a formalisation of the Rayleigh method, and that by reducing the variables to dimensionless ratios the total number of variables can be reduced. The method shown by Pritchard (pp.296-301, 2011) was used to form four Dimensionless Pi groups as shown in 3.2.2. An additional parameter is the Number of holes, which is itself a Pi group due to the fact that it is already dimensionless.

3.2.2 Defining Pi Groups

From section 3.1 it is apparent that the most important parameter affecting the validity of the hoverboard concept is the pressure drop through the system (ΔP). It is reasonable to assume that should this pressure drop be too great between the inlet and the cavity underneath the air cushion, then the lift force will be insufficient to generate an air cushion. With this key variable defined, the following relationship was proposed:

$$\Delta P = f(V, P, D_1, D_2, \rho, \mu, N)$$

$\Delta P = \text{Pressure Drop}$	$V = \text{Inlet Velocity}$	$P = \text{Inlet Pressure}$	$N = \text{Number of holes}$
$D_1 = \text{Hole Diamter}$	$D_2 = \text{Dist. from C/L}$	$\rho = \text{density of air}$	$\mu = \text{Dynamic viscosity}$
$\pi_1 = \frac{\Delta P}{P}$	$\pi_2 = \frac{D_2}{D_1}$	$\pi_3 = \frac{\rho V^2}{P}$	$\pi_4 = \frac{V\mu}{PD_1}$

Figure 3-8 Dimensionless Pi Groups

Which can be written in the form:

$$\pi_1 = f(\pi_2, \pi_3, \pi_4, N)$$

$$\frac{\Delta P}{P} = f\left(\frac{D_2}{D_1}, \frac{\rho V^2}{P}, \frac{V\mu}{PD_1}, N\right)$$

In order to establish a trend for each of the parameters, at least three variations for each condition are required. This generates a requirement for 21 fluid simulations to be run. All simulations have been run with air modelled as an incompressible fluid and therefore ρ will remain constant for all simulations. The parameters assigned for each of the 21 simulations are given in Appendix B.

For each Pi Group a single variable has been altered 3 times so that the effect of that change can be plotted. As well as modifying the variable 3 times, each Pi Group has been modelled for 3 different N values so that a curve for each value of N may be generated on the same plot.

In some instances it is possible to reuse the same geometric model to assess two different Pi Groups. Pi Group 1 will be plotted along the y-axis for each simulation as this is the variable that is of most importance. Each of the other Pi Groups will be plotted along the x-axis on a separate graph.

3.2.3 Summary

The fluid flow system of the hoverboard has been reduced to four dimensionless Pi groups which will be used to compare the characteristics of the flow when variables are changed. These groups were found using Buckingham's Pi Theorem and 21 different simulation models were generated using Solidworks.

3.3 CFD Simulation

In order to calculate the effects of varying the geometric properties in the hoverboard model, CFD simulation was undertaken using ANSYS 15.0 CFX at the University of Southern Queensland. The following section highlights the pre-processing methods and assumptions used during the simulation process.

Pre-processing involves defining the computational domain, subdividing the domain into appropriate control volumes, assigning fluid properties and specifying boundary conditions.

3.3.1 3-D Model

The 3-D model was produced in Solidworks using the dimensions listed in section 3.1.1 and in Appendix B. These models were then imported into ANSYS 15.0 for the fluid simulation studies.

A skirt with a “deformed” base was modelled to more accurately simulate the cushion design. It is reasoned that due to pressure variations across the bottom of the skirt, the cushion will not stay in its’ “ideal” modelled state, but is more likely to deform to the shape shown in Figure 3-9.

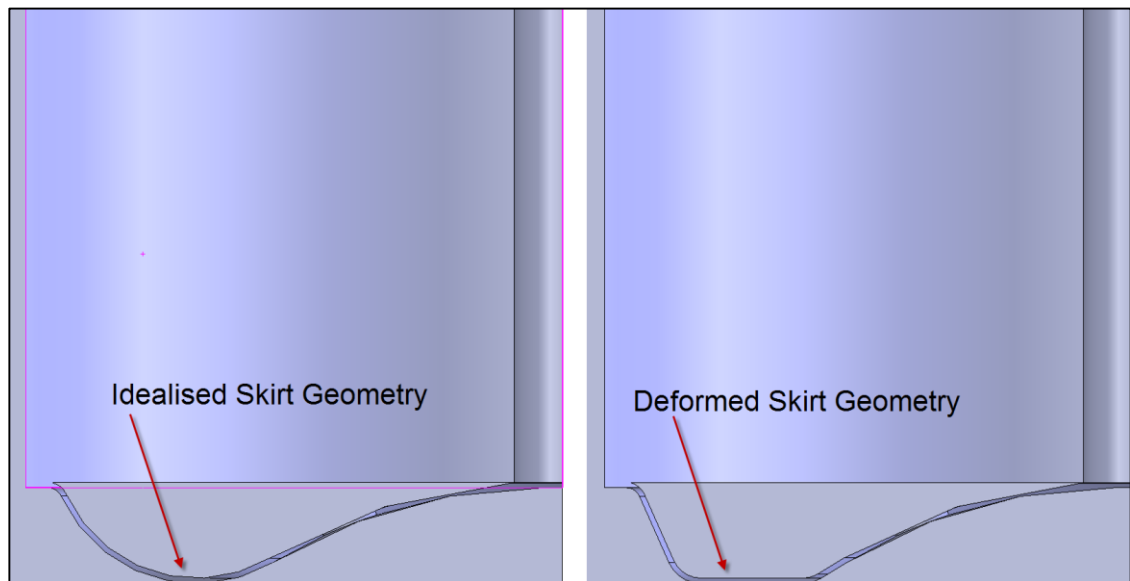


Figure 3-9 Skirt profiles

The deformation of the skirt allowed the CFX model to solve more accurately, as rather than having a tangency point with minimal contact, it allowed multiple elements to be established over this region and therefore generate a more fully developed flow. Not only did this allow for more robust simulations, but the deformed cushion is expected to more closely represent the actual profile of the cushion when it is in use.

A large control volume was created for the region after the air exits from underneath the skirt of the board. This was to reduce the effect of the outlet boundary condition on the solution, especially if there was any recirculation that occurred at the outlet. The total domain volume modelled for the CFD simulations was 1 m x 1 m x 0.5 m which allowed at least 500 mm from the exit.

Initial simulations were run with an air gap of 3mm, and these found that the pressure reached under the skirt was significantly lower than the minimum required 7000 Pa as outlined in section 3.1.1. To determine the maximum height at which the board may hover while maintaining 7000 Pa under the skirt, a series

of models was created. Each of these models had a varying air cushion gap and was run through the same simulation parameters. The average air cushion pressure was monitored and recorded, and this data was used to generate a curve relating skirt pressure to gap height h . Four models were used to generate the data points and these models were at 1mm, 0.5mm, 0.25mm, 0.13mm cushion height. The results of this initial simulation indicated that an air gap of just 0.16mm should be used. Detailed results and discussion of this process are presented in detail in Chapter 4. This cushion height was then applied to each of the consecutive models that were used to determine the Pi Group relationships.

3.3.2 Meshing Structure

Initial simulations were run using a coarse mesh of 300,000 – 350,000 tetrahedron elements. This simple geometrical mesh, shown in Figure 3-10, allowed for multiple simulations to be run while pre-processing debugging occurred. . The mesh had a growth ratio of 1.2 and minimum element size of 7.4766×10^{-4} m and a maximum element size of 0.149530 m.

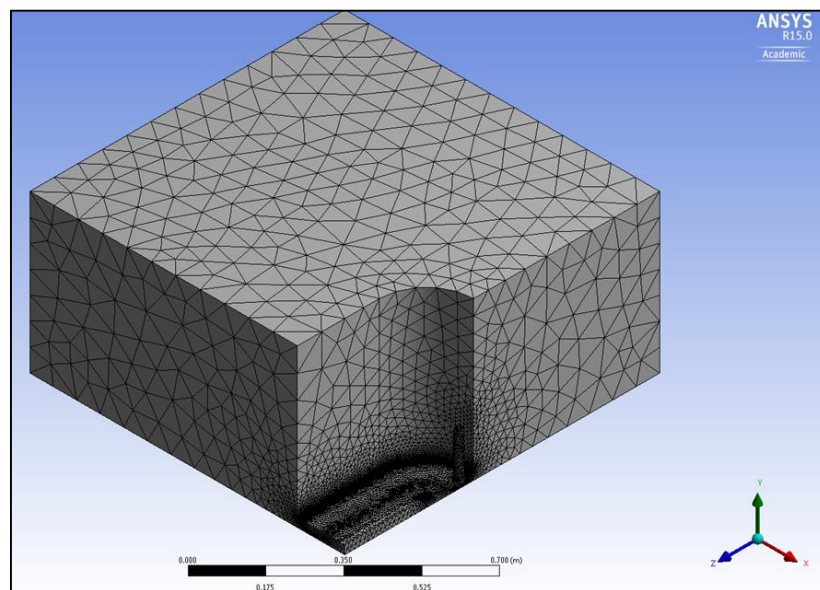


Figure 3-10 Preliminary Mesh

This mesh allowed for only 1 element through the thickness of the thin air cushion layer. This provided a stable model but did not allow for boundary effects to occur underneath the skirt. Given the extremely small gap that was simulated, obtaining a suitable mesh density through the boundary layer was difficult due to the number of nodes required in this region. The large number of nodes significantly increased the processing requirements of the study to the point that the computers used were unable to generate a mesh. This lack of elements through the small region is a limitation to this study. Numerous simulations were conducted with the air gap h being varied so that the pressure under the skirt could be established.

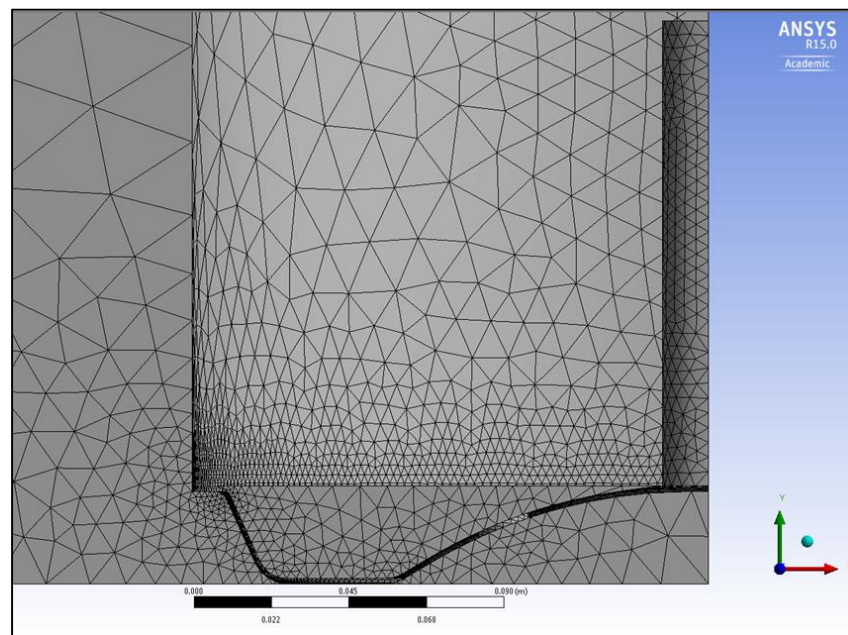


Figure 3-11 Side view of preliminary mesh

To determine the effects of the single element layer through the air gap a mesh independence study is required. A mesh independence study refines the mesh and uses the same simulation parameters to determine the effect of the mesh quality on the results presented. A number of different meshing refinement however a successfully refined mesh could not be achieved and simulated. This is thought to

be due to the sheer number of elements required in this region. If 5 elements were used through the section, each element would need to be 2.0×10^{-5} m in depth. If cubic elements were used for the entire air gap region, which had a volume of 2.49365×10^{-7} m³, then an order of elements approaching 31×10^6 would be required. This far exceeded the processing capabilities of the computers available.

It was reasoned that any variation between the results from the refined mesh and the coarse mesh will be acceptable. This is because the purpose of the study was to reduce pressure losses between the inlet and the skirt by modifying key parameters, and not to calculate the exact pressure losses of the system. By using the same coarse mesh for each of the simulations, valid comparative results for reducing pressure drop through the system could still be obtained.

3.3.3 Fluid Properties

The reference pressure for the simulation was set to 1 atm. In CFX, this is the pressure which all other boundary conditions are calculated relative to. Incompressible flow has been assumed because Pritchard (pp. 244) states that air flows with a Mach number of less than 0.3 can be assumed to be incompressible as they will experience a density change of less than 5 percent. In the simulation In all simulations Air was specified as an ideal gas and adiabatic conditions applied.

3.3.4 Boundary Conditions

Boundary conditions are necessary to solve the governing equations of the fluid dynamics equations over the given domain. These conditions define how the air behaves at these points and are used to establish the dynamics of the flow

throughout the rest of the model. These boundary conditions are specified for particular locations throughout the model, as shown in Figure 3-12.

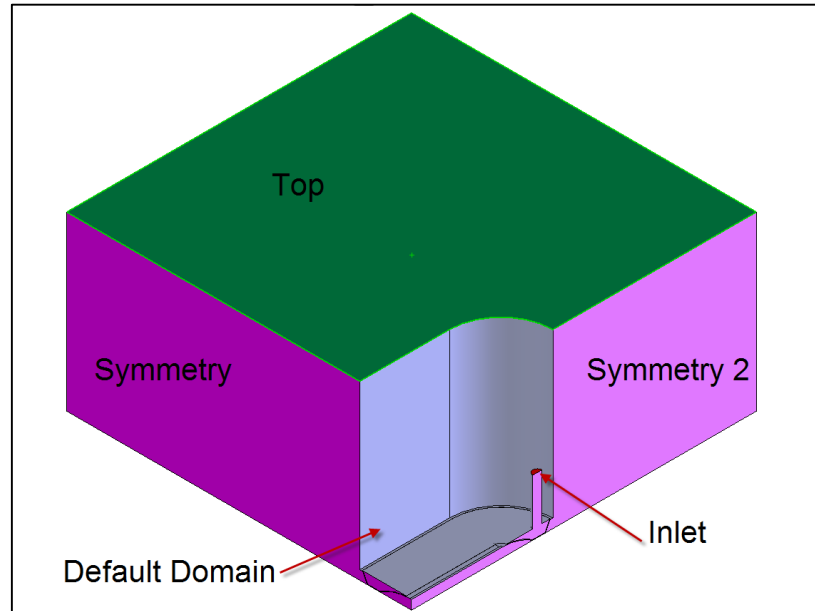


Figure 3-12 CFD Simulation Domains

Boundary conditions were specified at the inlet, outlet and all surfaces that came into contact with the fluid. Each study had varying parameters but maintained the same boundary conditions throughout. The only exception to this was the inlet diameter and inlet velocity boundary conditions which were changed so that Pi Group 4 parameters could be changed. It is recommended in the *Introduction to CFX (slides 24-39)* that the most robust boundary combination is a velocity inlet and static pressure outlet. This combination was used to help ensure an accurate and robust fluid simulation.

The standard inlet created was 54 mm in diameter and 135mm long. A length of 2.5 times the diameter ensured that the flow was fully developed before entering the skirt volume. The inlet velocity was specified as 2.5 m/s which gave a volumetric flow rate of $0.01156 \text{ m}^3/\text{s}$. This was the velocity and inlet diameter that were used for the majority of the simulations. Velocities at 2 m/s and 3 m/s were

also carried out and these simulations used inlet diameters of 49.5 mm and 60.7 mm respectively. Appendix B gives the parameters used for each Pi group model, and shows which simulations were run with different inlet velocity conditions.

A turbulence of 10% (High Intensity) was set at the inlet boundary condition and this was due to the highly turbulent flow that would be generated by a blower.

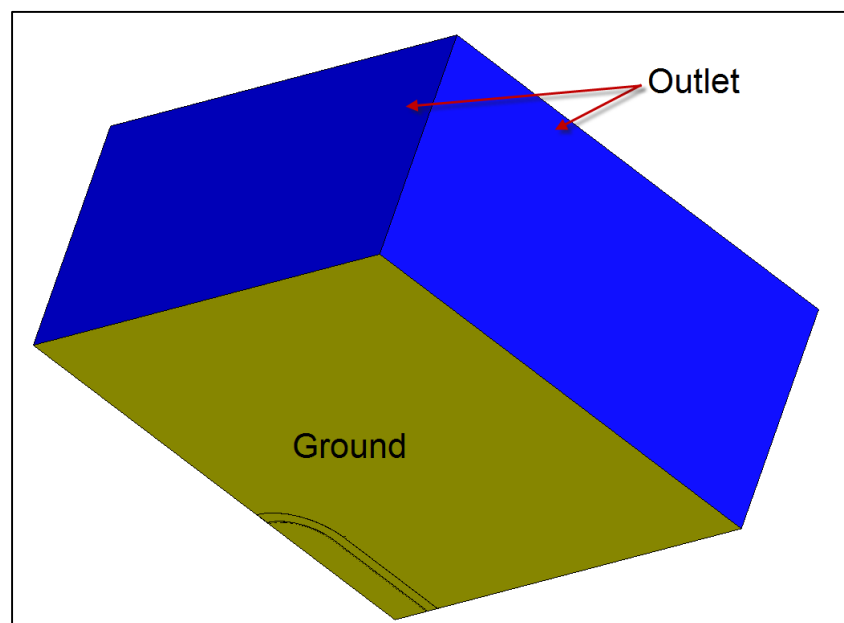


Figure 3-13 CFD Simulation Domains

An Outlet, shown in Figure 3-13, was specified with a static pressure of 0 Pa relative to the reference pressure of 1 atmosphere. This meant that the two outlet walls were at 101,325 Pa absolute pressure. It should be noted at this point that in the CFX program an *Outlet* boundary condition only allows flow out of the control volume, and does not allow air to flow back into the control volume should regions of low pressure develop. The top surface of the domain was set as a wall with free slip. In reality this surface would also be atmospheric, however the CFD simulation became unstable when this was set. By making this surface a free slip

wall, very little impact was made on the fluid flow due to the surface being 500 mm above the bottom of the air cushion where the flow of interest was occurring.

The ground surface was defined as a wall with a no slip condition and a sand grain roughness of 0.5 mm. This sand grain roughness value was an assumed amount based on the roughness of concrete proposed by Pritchard (p 359). The default domain covered all remaining surfaces in the fluid model and was characterised as a no slip wall with a sand grain roughness of 0.25 mm, which was again an assumed value based on the data given by Pritchard.

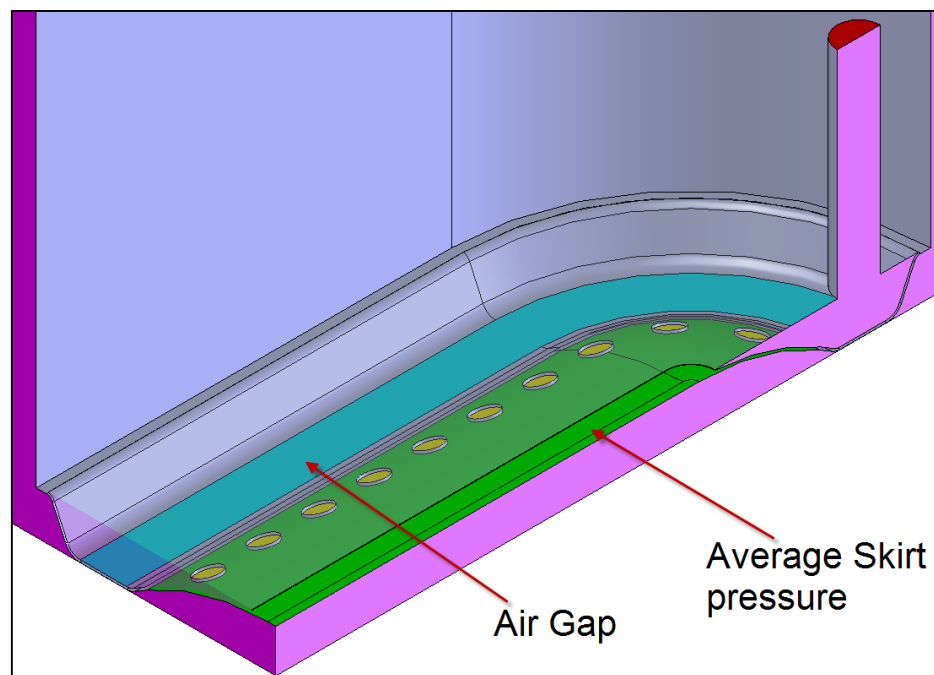


Figure 3-14 CFD Simulation Domains

There was also an Air Gap domain and an Average Skirt Pressure domain that was specified as shown in Figure 3-14. These regions were specified for monitoring the air velocity out under the skirt and the average skirt pressure available to develop a lift force on the underside of the board.

Two symmetry planes were used to reduce the amount of elements in the simulation by 75%. These symmetry planes were placed through the centre of the board and perpendicular to the Deck. A summary of the boundary conditions used are presented in Table 3-3.

Boundary Name	Condition Specified
Inlet	Uniform Velocity Inlet
Outlet	Static Pressure Outlet
Symmetry	Symmetry
Symmetry2	Symmetry
Ground	Wall, no slip, sand grain roughness of 0.5mm
Top	Wall, free slip
Default Domain	Wall, no slip, sand grain roughness of 0.25mm
Air Gap	Wall, no slip, sand grain roughness of 0.25mm
Average Skirt Pressure	Wall, no slip, sand grain roughness of 0.25mm

Table 3-3 Boundary Conditions for Fluid Simulation

3.3.5 Simulation Solver

The solving stage of the fluid simulation process requires inputs regarding the number of iterations, the initial conditions and convergence criteria.

The *ANSYS Solver Theory Guide* (2009, pp. 18-26) lists the complex governing equations used implicitly by the solver to generate the fluid simulation results. The solver plots the root mean square (RMS) error for each of the key equations which are; the momentum equation, the mass density equation, the continuity equation, the transport equation, the thermal energy equation and the equations of state. One key indicator of the models robustness at this stage of the simulation is that the solver converges the Root Mean Squared (RMS) error of these governing equations to a value of less than 1.0×10^{-4} . This value of RMS error is

generally accepted to be a reasonable value. An RMS error tolerance helps to ensure the accuracy of the model and generally allows any abnormalities to present themselves prior to generating a result. However for the simulations conducted an RMS convergence tolerance of 1.0×10^{-6} was used. This was because the monitored value of average skirt pressure had not reached an acceptable steady state condition at the RMS tolerance of 1.0×10^{-4} . To achieve steady state conditions in the monitored pressure values, the maximum number of iterations for each simulation was set to 1250. Through experience in the pre-processing and initial simulation runs, it was determined that 1250 iterations was sufficient to allow the RMS errors to converge on the required tolerance.

The initial conditions for the simulations are the first guess that the program uses when solving the governing equations implicitly. This function was set to the “Initial Conditions” setting, which involves the CFX program taking a guess at the first set of values based on the boundary conditions and domain information that has been input. Specifying closer initial conditions can shorten the run time of a simulation however this was not practical for these simulations. The simulation time for each instance was acceptable with the “Initial Conditions” setting.

Monitor points were included for post processing however these were also useful in ensuring the validity of the model. Monitor points were included in the pressure region underneath the skirt so that average pressure values could be obtained. Ensuring that the monitor points had reached a steady state solution by the end of the simulation was an excellent indication of the accuracy of the model. The average skirt pressure was monitored during each simulation to ensure that a steady state level of $\pm 10\%$ was achieved. This was the case by the time each

simulation had reached 1250 iterations. The monitored values generally took on a form similar to Figure 3-15.

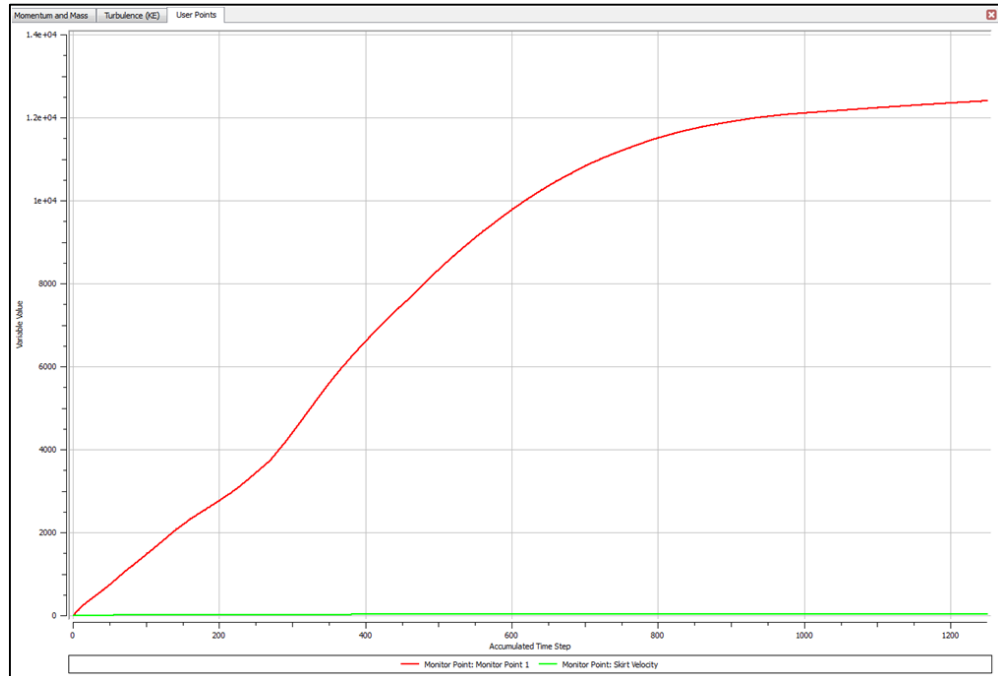


Figure 3-15 Sample of Steady State conditions for monitored values

Some limitations with the solver were the significant variation between mesh sizes that were required. For the small air cushion layer, element sizes of 1.6×10^{-4} m were required, while in the outer regions of the domain elements up to 0.15 m were used. This drastic change in element size caused some issues with the element growth ratios and caused many mesh failures. A further limitation to the study is the lack of a mesh independence study as mentioned previously.

3.3.6 Post Processing Simulation Data

Post processing involves the manipulation of the data files created during the simulation. These data files must be converted into useful results through the use of programs such as Microsoft Excel and Matlab. The data from the CFX simulations was post-processed in Microsoft Excel.

Preliminary Histogram plots were generated for each simulation which showed the pressure distribution over the skirt area. Additional plots which showed the pressure distribution over the inlet area were also generated. These allowed the average pressure for that region to be calculated, and this average pressure value was input into excel to generate the graphs used in Chapter 4.

These averaged values were also then used to plot the Pi Group curves shown in Chapter 4. Given that the pressure drop over the system is the key objective of this report, the area of focus for post processing data was the area under the skirt cushion A_p . These values were averaged to produce an approximate lift force on the board.

3.3.7 Model Validation

Validation is necessary to confirm any numerical or simulation model. Generally this validation occurs in the form of comparisons between simulation data and experimental results. If the output of the model is considered to be similar to the experimental results within a defined tolerance, then the model may be considered appropriate for use. Due to the unique nature of this project no experimental data is yet available to confirm the results of the model. The acquisition and comparison of this experimental data has been restricted by time constraints and is described in detail in Chapter 5.

3.3.8 Limitations of Use

There are numerous limitations to the use of this fluid model which are discussed in detail in Chapter 4. The results generated from this study provide a foundation for further research and validation experiments.

3.4 Summary

Chapter 3 has presented the methodology used to undertake Computational Fluid Dynamic simulation of an air powered hoverboard. The focus was to obtain reliable input data through experimental testing, and then to use this data to construct a valid CFD model. This model then combined dimensional analysis with CFD to investigate a skirt design which would reduce pressure losses between the inlet and the board lift area, thereby reducing the net power requirements of a battery operated hoverboard.

Average pressures under the skirt were extracted from 21 fluid simulation studies and plotted as a series of Dimensionless Pi Groups so that the key relationships between parameters could be established.

Chapter 4

Results and Discussion

Chapter 4 presents the results achieved when the methodology from Chapter 3 was applied, and discusses the strengths and weaknesses of these results. This chapter presents a general overview of the results of each simulation, critical analysis of the results achieved and the expected and unexpected results obtained. These results are then compared with the results presented by Shan et al. (2008) and variations between the two are discussed. A discussion on the limitations for the use of these results is presented along with potential improvements that arise from the results.

4.1 General Statements of Results

This section presents the key outcomes as they were obtained. These results follow the methodology process and are listed in this order. Data obtained from CFD simulations has been reduced to more reader friendly format and is presented in the form of graphs and tables showing key values.

4.1.1 Idealised Skirt vs Deformed Skirt

Initial simulations were conducted under the assumption that the skirt would maintain its ideal shape and the radius of the cushion would not deform under pressure. Each of these simulations generated very similar average skirt pressures

regardless of cushion height or hole configuration. The maximum pressure generated in these simulations was 54 Pa and occurred at a 0.05mm gap. After these simulations were run the results were determined to be unrealistic and the model was changed to the deformed base style as shown in 3.3.1 on page 38.

4.1.2 Cushion Height vs Skirt Pressure

One of the first issues encountered with the CFD simulation was that the pressure under the skirt was too low to generate lift when the given boundary conditions were input. Initial height values ranged from 0.1 mm to 3 mm in 0.5 mm increments. The peak pressure obtained by simulations over 1 mm was 70 Pa gauge. This is significantly under the minimum required amount of 7 kPa which was determined in section 3.1.1. In order to establish the maximum hover height h at which the skirt pressure was still above 7 kPa a series of simulations were run with varying air gaps. At the completion of each of these simulations two histograms were generated from the simulation data, a sample of which is shown in Figure 4-1

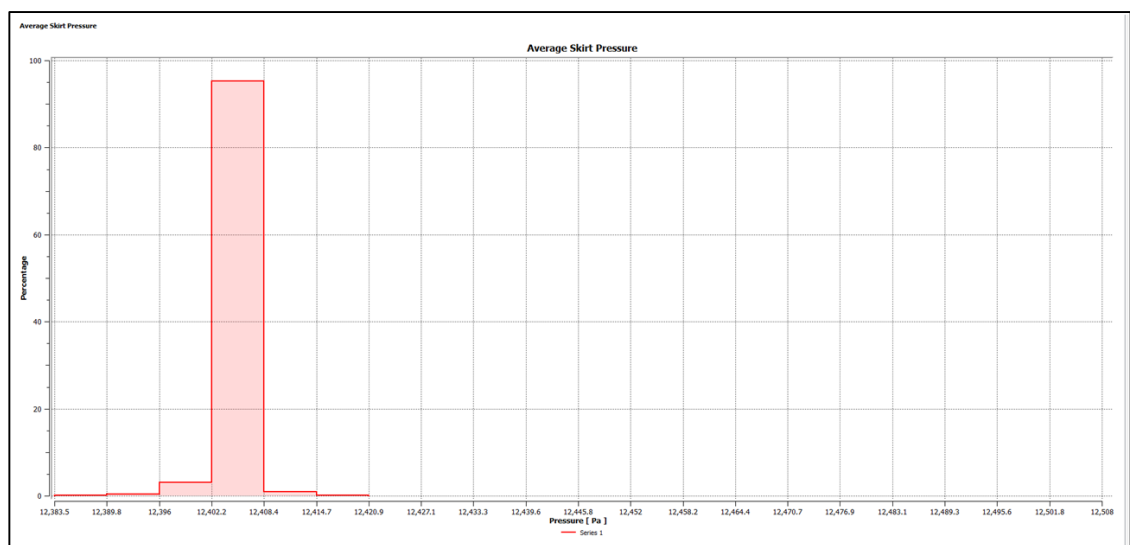


Figure 4-1 Sample Histogram plot of pressure over "Average Skirt Pressure" domain

The first of these Histograms showed the pressure in the “Average Skirt Pressure” domain, grouped by percentage of area. These plots were generated for all simulations and a sample of these is included in Appendix D. A similar histogram plot was generated which showed the Inlet pressures grouped by percentage area.

The average skirt pressure from these results was then plotted in Figure 4-2 to show the variation in pressure with air gap.

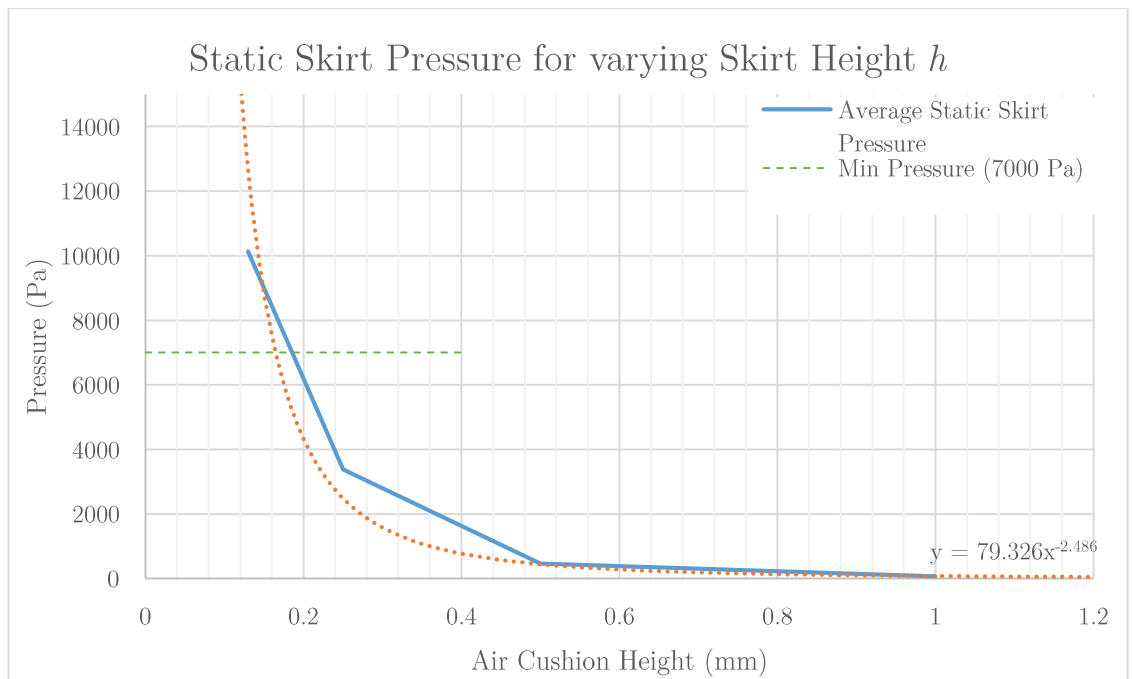


Figure 4-2 Plot of Skirt pressure for varying air cushion heights in preliminary simulation configuration

A line of best fit was plotted through these points to generate an equation for the relationship between board height h and skirt pressure P_{skirt} . It is proposed that this relationship can be modelled as

$$P_{skirt} = 79.326 \times h^{-2.486}$$

This relationship is only valid for the preliminary model that was used in the approximate air hover gap simulations.

This model had the parameters of as specified below:

$$N = 30,$$

$$D_1 = 8 \text{ mm}$$

$$D_2 = 110 \text{ mm}$$

Once the optimum configuration was selected this study needed to be recreated with the new parameters. A new plot and relationship can then be proposed which would more accurately represent the relationship between board height and skirt pressure for experimental testing.

The pressure distribution contour plot produced trends that coincided with predicted results. The peak pressure values were at the inlet, and then a slight pressure drop occurred as the flow travelled from the inlet to inflate the skirt. There was then a further pressure drop as the air flowed through the skirt outlet holes into the region underneath the board. The pressure drop through these holes is an essential part of the cushion design. If there was no pressure drop through this section then there would be a risk that the skirt would not inflate and therefore not work as designed.

By maintaining a slightly higher pressure internally the skirt is guaranteed to always be inflated based on Pascals Law:

$$\textit{Force} = \textit{Pressure} \times \textit{Area}$$

Pressure stabilisation occurred in the region underneath the board that generates the lift force P_{min} , before decreasing down to atmospheric pressure as the air flows out under the skirt into the outlet control volume. It can be seen from Figure 4-3

that the largest pressure variation occurs between the cavity under the board and the atmospheric control volume.

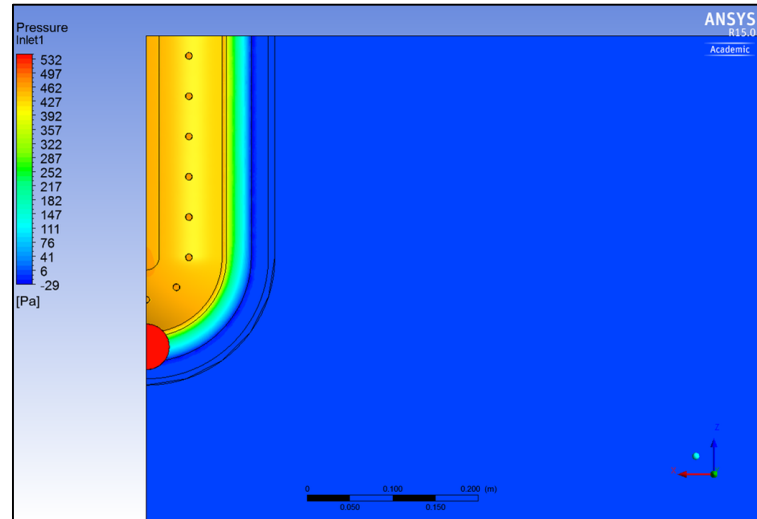


Figure 4-3 Top View of Pressure Distribution Plot on Inlet, Average Skirt Pressure and Ground Domains for $h=0.5\text{mm}$ preliminary simulation

This pressure profile was consistent between simulations. While the pressure values varied between simulations, the general trends remained the same. For this reason only a single pressure contour plot will only be shown. Figure 4-4 provides a view from underneath of the pressure distribution plot.

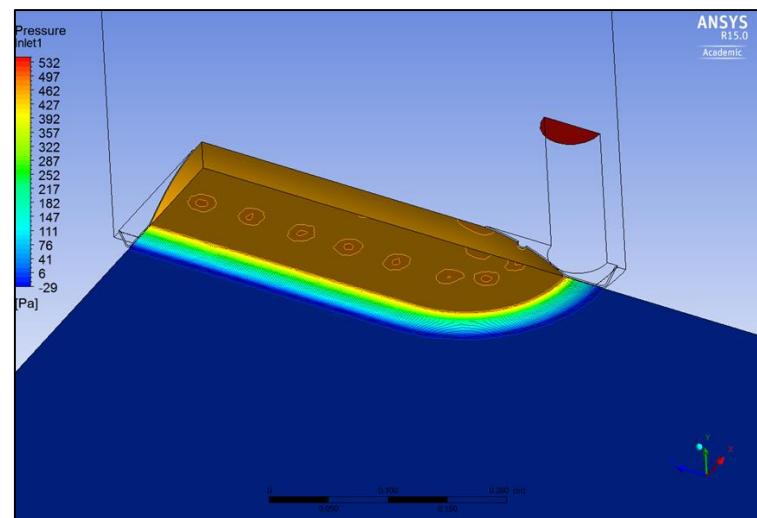


Figure 4-4 Underside view of Pressure Distribution Plot on Ground, Average Skirt Pressure and Inlet domains for $h=0.5\text{mm}$ preliminary simulation

This image highlights the small pressure variation that occurs along the ground domain where the air exits the skirt outlets and hits the ground. This pressure variation is caused by the additional dynamic pressure that is associated with these streams of air. These regions experience a much higher dynamic pressure than the rest of the region which is mostly subjected to static pressure.

A side view of the velocity profile through the board is shown in Figure 4-5. This velocity profile shows that the air enters the simulation at the velocity specified in the boundary conditions. It is important to check that this is occurring to ensure that the boundary conditions are functioning as intended. As expected there is thoroughly turbulent flow throughout the simulation, largely caused by the irregular geometry. The velocity decreases as the air enters the skirt and travels to the skirt outlet holes.

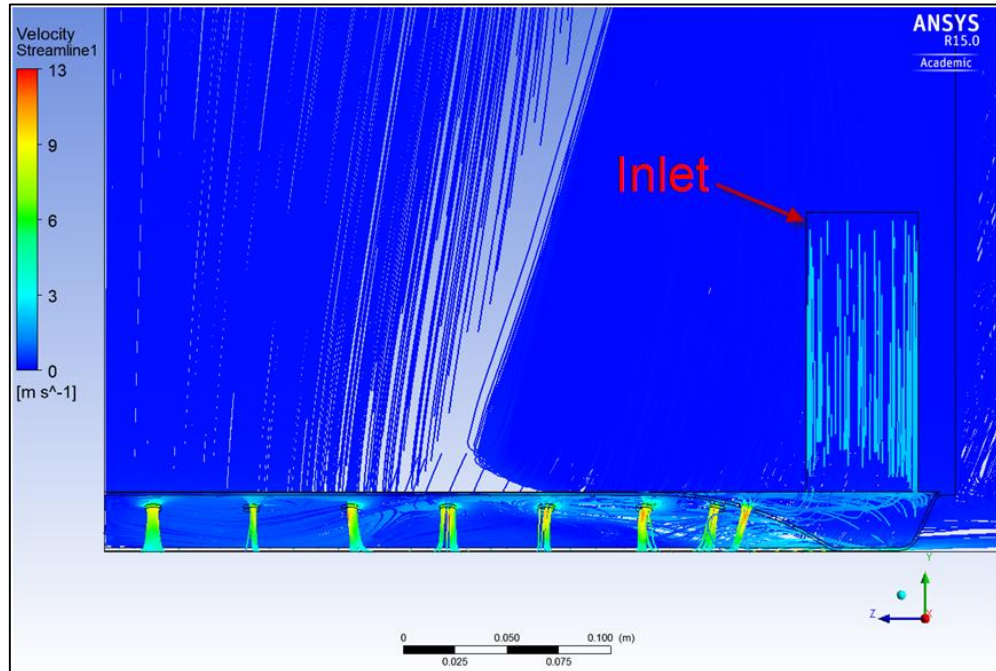


Figure 4-5 Side View of Velocity Streamlines for $h=0.5\text{mm}$ preliminary simulation

At the skirt outlet holes the velocity increases significantly over a very small distance. This rapid velocity increase is what generates the pressure drop through

these holes which confirms the form of Bernoulli's equation listed in Pritchard (pg 14):

$$\frac{P_1}{\rho} + \frac{V_1^2}{2} + gz = \frac{P_2}{\rho} + \frac{V_2^2}{2} + gz = \text{constant} \quad \text{Equation 4-1}$$

It can be seen that the streamlines in Figure 4-5 correspond with the localised high pressure regions shown in Figure 4-4 which confirms that the dynamic pressure from the air streams is what causes these pressure variations on the ground domain. These variations are not significant enough to affect the operation of the hoverboard.

The streamline plot shown in Figure 4-5 does not clearly highlight the effects of the air cushion on the velocity profile. In Figure 4-6 this velocity profile is shown in more detail.

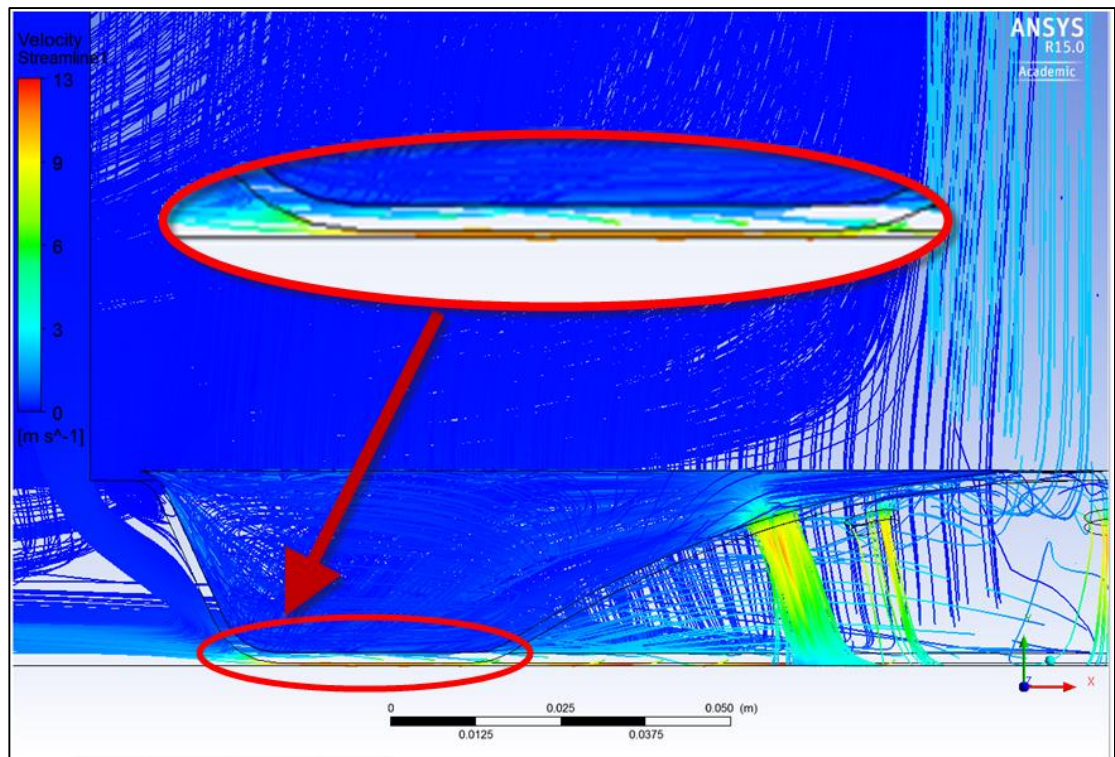


Figure 4-6 End View of velocity streamlines for h=0.5mm preliminary simulation
INSET - Velocity streamlines through air cushion

It can be seen that the peak velocity for the simulation occurs in this region. The air rapidly accelerates to 13 m/s as it passes through the 0.5 mm air cushion. In all of the preliminary simulations the velocity through the air cushion remained below 103 m/s and therefore remained in the region of incompressibility for the purpose of this study. The control volume outside of the skirt was deemed to be large enough to make any effects on the internal simulation negligible. Figure 4-7 indicates with a red arrow that the flow out from the skirt has become laminar and the velocity has decreased. It can also be seen that some recirculation is occurring in the domain outside of the skirt. It is likely that this is due to a low pressure (negative to the reference pressure) region inside the domain, which does not let the air flow past the outlet. This effect is not thought to have impacted on the results of interest in the study.

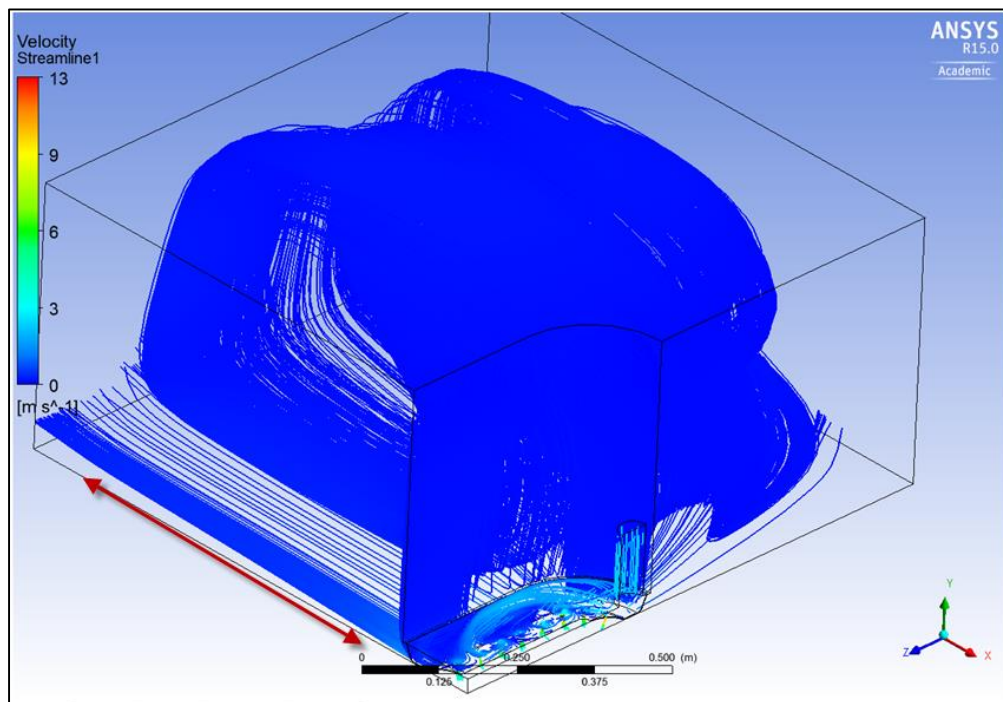


Figure 4-7 Isometric View of velocity streamlines for $h=0.5\text{mm}$ preliminary simulation

4.2 Pi Group Relationships

This section will highlight the relationships that were found between each of the dimensionless Pi Groups and discuss what these relationships mean. It will list the results of the 21 CFD simulations and discuss their relationships.

4.2.1 Pi Group 1-2 relationship

The first series of simulations were run to establish the relationship between Pi Groups 1 and 2 which are $\frac{\Delta P}{P}$ and $\frac{D_2}{D_1}$ respectively. The parameter that was varied was D_2 which is the distance between the axis of the outlet holes, symmetric about the board centreline. This parameter is defined more clearly in Appendix C which shows the detailed board dimensions used for the calculations.

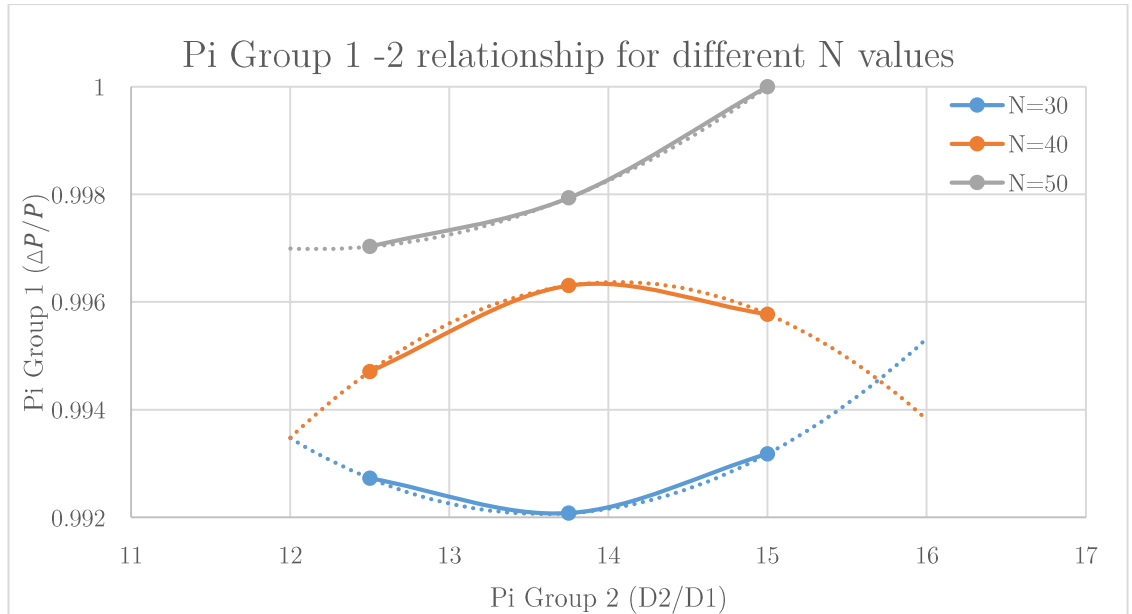


Figure 4-8 Relationship between Pi Groups 1 & 2 for three values of N

It can be seen in Figure 4-8 that the relationship between Pi Group 1 and 2 have been plotted for three values of N . This graph clearly shows that the impact of varying the relationship between D_2 and D_1 is negligible, as the pressure drop

through the system is less than 1% for all 9 configurations that were simulated. What this graph does indicate however is that of the three Pi Groups simulated (Pi Group 1, 2, and N), the number of holes N was the most influential factor in determining pressure drop. As the number of holes increased, the pressure drop decreased. This is in accordance with Bernoulli's equation:

$$\frac{P_1}{\rho} + \frac{V_1^2}{2} + gz = \frac{P_2}{\rho} + \frac{V_2^2}{2} + gz = \text{constant} \quad \text{Equation 4-1}$$

because a larger number of holes would increase the area through which the fluid flows. This increased area would mean that the velocity of the air would not accelerate as much when passing through the skirt outlet holes.

This is based on the assumption that $Q_{in} = Q_{out}$ and recalling from section 3.1.3 that

$$V_{out} = \frac{Q_{out}}{A_{out}}$$

As can be seen the velocity will decrease as area increases, and this same relationship was reflected between N and Pi Groups 1 and 2.

It is recognised also that the results for $N = 40$ appear to diverge slightly from the $N = 30$ and $N = 50$ lines. It is possible that some margin of error has been introduced. To re-assess this a further 2 or three simulations could be run which would more clearly define the trend of that line and give a clearer indicator if this was a correct value or an outlier. Due to time constraints with this study this further simulation has not been completed.

4.2.2 Pi Group 1-3 Relationship

The second series of simulations run were to establish the relationship between Pi Groups 1 and 3 which are $\frac{\Delta P}{P}$ and $\frac{\rho V^2}{P}$ respectively. This relationship was again plotted for 3 different values of N . To achieve these results 9 separate simulations were run and the parameter that was varied was the inlet velocity V . The inlet diameter was also altered for each of these simulations so that the volumetric flow rate between simulations remained constant at 0.01156 m³/s.

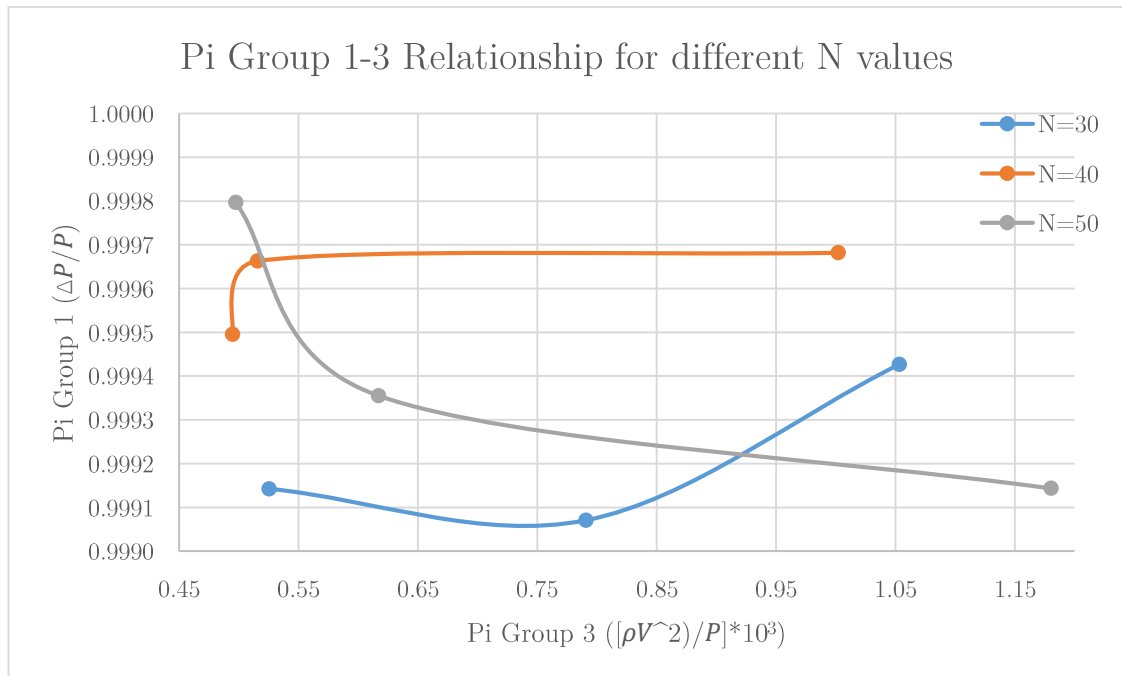


Figure 4-9 Relationship between Pi Groups 1 & 3 for three values of N

In Figure 4-9 the ratio of Pi Group 1 over Pi Group 3 has been plotted for 3 values of N . It should be pointed out that the values of Pi Group 3 on the x-axis have been increased by a factor of 10^3 to improve readability of the plot. This should be taken into account when specifying ratio values for this Pi Group. From this graph it can be seen again that higher values of N result in lower pressure losses and that the $N = 30$ range is the least effective. As the ratio of Pi Group 3 increases above around 0.92 the $N = 30$ configuration becomes more efficient than

the $N = 50$ configuration. For any Pi Group 3 ratios above 0.52, the $N = 40$ configuration is clearly the best option.

What Figure 4-9 highlights is that for $N = 50$ the increasing velocity actually decreases the efficiency of the system. This is likely due the nature of the $\frac{v^2}{P}$ relationship, such that if the velocity is increasing, the inlet pressure is likely to decrease. However this Velocity term is squared and therefore Pi Group 3 will vary much more significantly with increased velocity than Pi Group 1 will from the corresponding pressure change.

4.2.3 Pi Group 1-4 Relationship

The final series of simulations were run to establish the relationship between Pi Group 1 and Pi Group 4 which are $\frac{\Delta P}{P}$ and $\frac{V\mu}{PD_1}$ respectively. The parameter that was varied was D_1 , which is the skirt outlet hole diameter. Results from previous Pi Group simulations were re-used to generate the data for this Pi Group relationship, meaning that only 3 additional models were required.

It is shown in Figure 4-10 on page 63 that this relationship has been plotted for 3 different values of N . What can be seen from this plot is that for the range of $40 \leq N \leq 50$ the efficiency is very similar for Pi Group 4 values of 0.01 to 0.03. It is only for Pi Group 4 ratios greater than 0.03 that the number of holes makes a noticeable difference. The efficiency of the $N = 30$ hole configuration peaks at about this same Pi Group 3 ratio of 0.03.

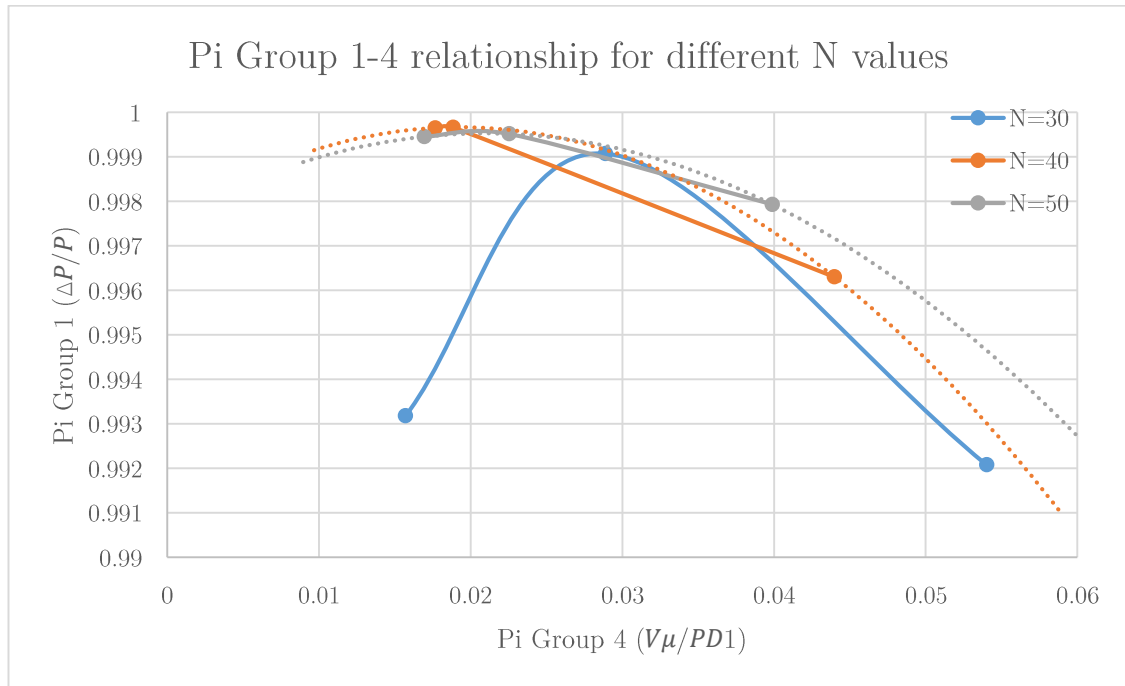


Figure 4-10 Relationship between Pi Groups 1 & 4 for three values of N

Given how rapidly the pressure efficiency decreases when Pi Group 3 ratios exceed 0.03, it is clearly a key parameter that should be adhered to when designing the final configuration.

4.3 Optimum Configuration

To select the optimum configuration the ideal ratios for each Pi Group relationship have been selected based on the trends displayed. These ratios are:

$$\text{Pi Group 2} - \frac{D_2}{D_1} = 15 \quad \text{Equation 4-2}$$

$$\text{Pi Group 3} - \frac{\rho V^2}{P} = 0.005 \quad \text{Equation 4-3}$$

$$\text{Pi Group 4} - \frac{V\mu}{PD_1} = 0.02 \quad \text{Equation 4-4}$$

These relationships have then been rearranged and the known constant values of $\mu = 1.7894 \text{ kg/m} \cdot \text{s}$ and $\rho = 1.225 \frac{\text{kg}}{\text{m}^3}$ have been substituted in so that:

$$D_2 = 15D_1 \quad \text{Equation 4-5}$$

$$P = \frac{\rho V^2}{0.005} = 2450V^2 \quad \text{Equation 4-6}$$

$$P = \frac{V\mu}{0.02D_1} = \frac{89.47V}{D_1} \quad \text{Equation 4-7}$$

Then by substituting equation 4-6 into 4-7 it can be found that:

$$2450V^2 = \frac{89.47V}{D_1}$$

Which reduces to:

$$V = \frac{0.0365}{D_1}$$

Using these relationships Table 4-1 has been generated.

N=50	D1 (m)	V (m/s)	P (Pa)	D2 (m)	Pi 2	Pi 3	Pi 4
	0.005	7.30	130692	0.075	15	0.0005	0.02
	0.006	6.09	90758	0.090	15	0.0005	0.02
	0.007	5.22	66680	0.105	15	0.0005	0.02
	0.008	4.56	51052	0.120	15	0.0005	0.02
	0.009	4.06	40337	0.135	15	0.0005	0.02
	0.010	3.65	32673	0.150	15	0.0005	0.02
	0.011	3.32	27002	0.165	15	0.0005	0.02
	0.012	3.04	22690	0.180	15	0.0005	0.02
	0.013	2.81	19333	0.195	15	0.0005	0.02
	0.014	2.61	16670	0.210	15	0.0005	0.02
	0.015	2.43	14521	0.225	15	0.0005	0.02
	0.016	2.28	12763	0.240	15	0.0005	0.02
	0.017	2.15	11306	0.255	15	0.0005	0.02
	0.018	2.03	10084	0.270	15	0.0005	0.02
	0.019	1.92	9051	0.285	15	0.0005	0.02
	0.020	1.83	8168	0.300	15	0.0005	0.02

Table 4-1 Optimum Skirt Configurations

Table 4-1 shows the optimised board configurations for any given outlet hole diameter D_1 . Other factors to be considered in the selection of an optimum configuration are the physical dimensions of the board. Due to these physical dimensions the maximum allowable D_2 value is 150 mm. This means that the best configuration is the one highlighted in green in Table 4-1. The Pi Ratios for each of these configurations is also shown in this table.

4.4 Optimised Hover Height

Once the optimised configuration had been determined four simulations were run to establish a value for hover height h . This process was exactly the same as was conducted in section 4.1.2 except that the h values used in the simulation were 0.1 mm, 0.2 mm, 0.5 mm and 0.8 mm. The results of these simulations have been compared with the preliminary height simulation and are shown in Figure 4-11.

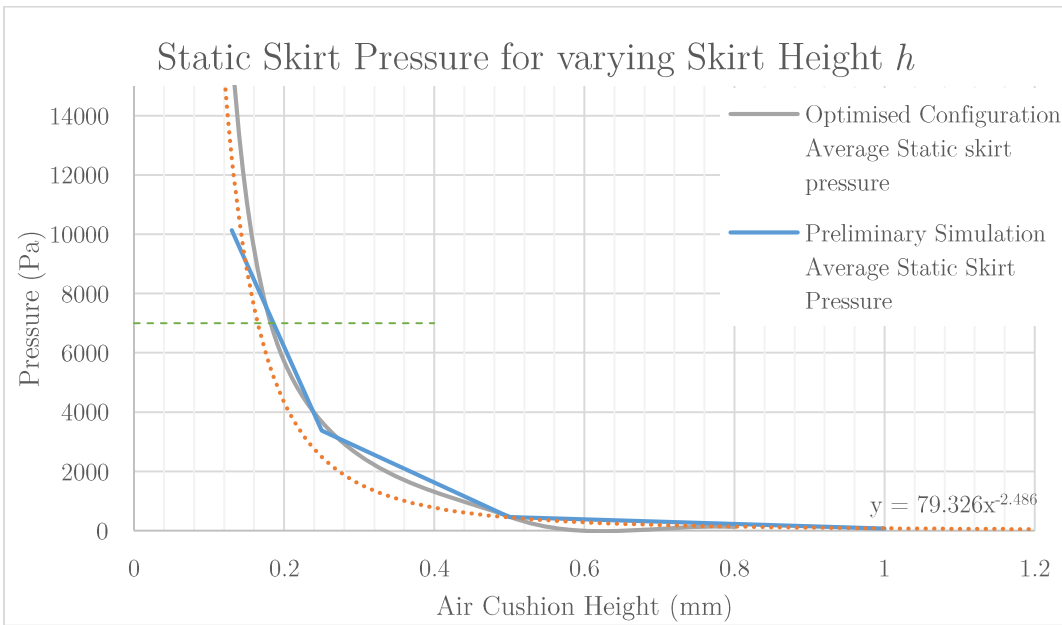


Figure 4-11 Optimised configuration Skirt Pressure for varying skirt heights

These results show that by optimising the skirt design the air gap has actually increased slightly. It is proposed that hover height is related to pressure by the new equation:

$$P_{min} = 79.326 \times h^{-2.486} \quad \text{Equation 4-8}$$

The optimum hover height at which $P_{min} = 7000 \text{ Pa}$ can then be found from Equation 4-8 to be 0.165 mm. A very similar trend to the preliminary simulations is seen which is to be expected with an improved design. A sample of the FEA reports generated by ANSYS CFX have been shown in Appendix D. All reports for all simulations were not presented as there was no benefit to providing the data when each simulation was run using the same conditions. This also applies to the Histogram plots showing the average pressure at the inlet and the under skirt pressure.

4.5 Previous Studies

In the paper presented by Shan et al (2008) the key results were that the optimum hole configuration to reduce air velocity standard deviation and pressure losses was 44 holes. This paper assumed an inlet velocity of 53.65 m/s which was in the region of incompressible flow, however it was much higher than the velocity used in this study. The results obtained in this study tend to confirm the general trends published by Shan et al (2008) in that the higher number of holes reduces pressure losses between the inlet and the cavity under the skirt. However the study published by Shan et al (2008) does not give any further detail regarding board dimensions and therefore additional comparisons cannot be fairly made.

4.6 Expected Results

There were a number of expected results in this study and also some unexpected ones. The expected results were that increasing the number of holes and hole diameter would decrease the pressure losses between the inlet and the cavity under the skirt. These expectations were confirmed with the CFD simulations. The results made sense as the larger area through which the fluid flowed meant that there would be less of a velocity increase. It has already been shown that velocity and pressure are related by the Bernoulli equation:

$$\frac{P_1}{\rho} + \frac{V_1^2}{2} + gz = \frac{P_2}{\rho} + \frac{V_2^2}{2} + gz = \text{constant} \quad \text{Equation 4-1}$$

It makes sense therefore that if the velocity increases then pressure decreases. Therefore if the velocity increases by a smaller amount, then conversely the pressure will decrease by a smaller amount and the pressure drop will be less.

One of the most unexpected results from the study was the height of the air cushion on which the board rests. Preliminary estimates based on the report of Shan et al. (2008) suggested that the air cushion height could be between 2 mm and 3 mm. The air gap estimated in the preliminary study section 3.1.4 proposed a minimum air gap of between 0.65 mm and 3 mm. This estimation was confirmed in section 4.4 where it was proposed that the board hover height for the optimum configuration would be 0.165 mm. This is significantly different from the 2 mm to 3 mm gap proposed by Shan et al. (2008). This discrepancy could potentially arise from different board geometry between the studies or from different volumetric flow rates and velocities used.

Chapter 5

Further Work

5.1 Prototype Testing

5.1.1 Construction

The validation of this project will require the fabrication of a prototype board and the use of an electric leaf blower for testing. Both of these tasks will involve some inherent risks that need to be controlled to ensure the safety of all people involved.

The fabrication phase of the Hoverboard will involve the use of some power tools such as Jigsaws, Cordless Drills and Belt Sanders. Various hand tools will also be used throughout the construction phase. The use of each of these tools will inherently contain hazards which need to be addressed in the form of a risk assessment prior to use. A risk assessment should be completed prior to undertaking any task. An example risk assessment has been completed and is shown in Appendix E. The risk assessment addresses all safety concerns and lists control measures to minimise any risk. The assessment should be conducted in accordance with AS/NZ ISO 31000:2009 Risk Management – Principle and guidelines.

5.1.2 Testing

In order to validate the CFD simulation, pressure readings will be required underneath the air cushion of the hoverboard. Due to the low air cushion gap, obtaining valid data may prove difficult. To help overcome this a possible testing configuration has been proposed in Figure 5-1 To measure the outlet velocity and pressure at each of the holes, a Pitot tube should be used in a test set up shown.

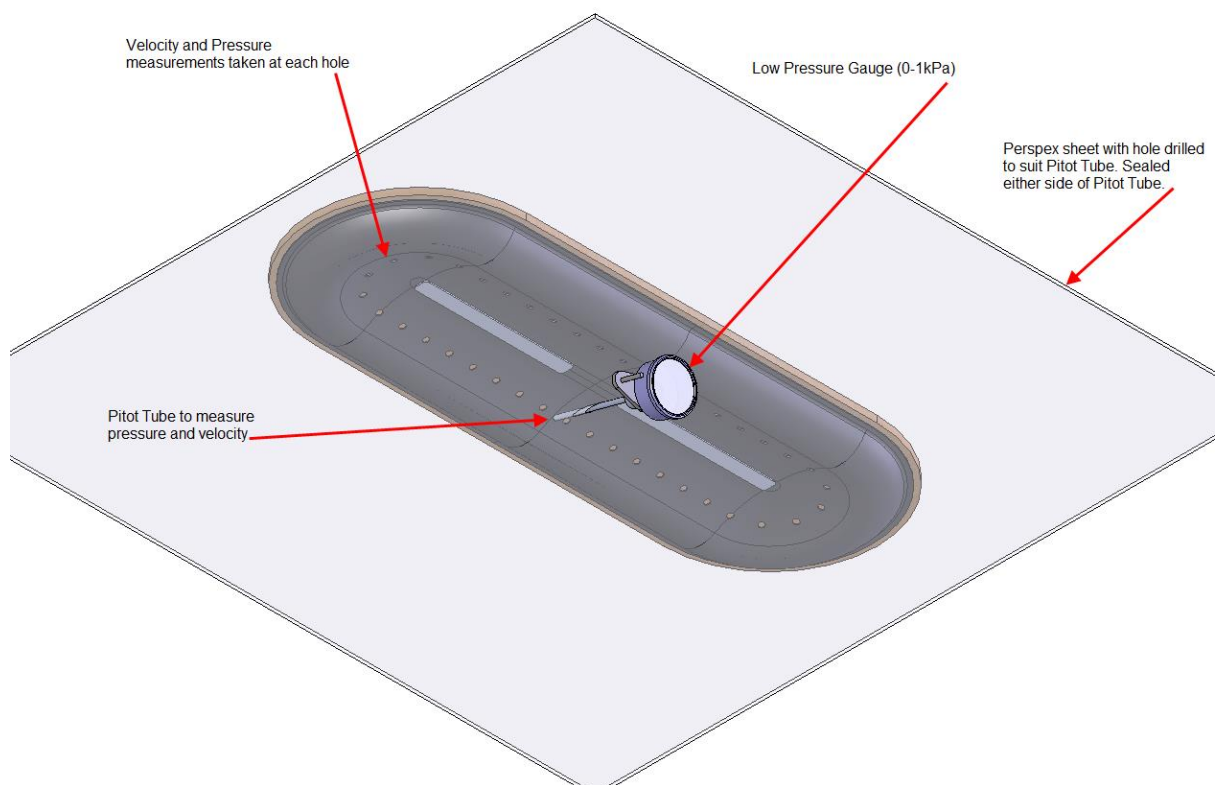


Figure 5-1 Possible Experimental Testing Setup

The Pitot tube should be mounted in the centre of a large Perspex sheet. The Perspex sheet is to be sealed around the Pitot tube so that air cannot escape through the hole. This will minimise the effects of the Pitot tube on the flow field and help ensure accurate results.

A leaf blower or equivalent source should be operated at the same volumetric flow rate and inlet pressure as specified in Chapter 3. If another power level is specified

then the Dimensional Analysis graphs listed in Chapter 4 should be used when comparing the experimental and CFD results. Once the board has reached steady state equilibrium in the experimental set up, it should be moved around the Pitot tube and pressure and velocity measurements taken at each hole.

5.1.3 Validation of CFD model

Once the experimental results have been obtained they should be checked to be dimensionally equivalent to the CFD results. Once this has occurred the results should be compared and any deviations between them highlighted. If the variation between the results is out by a constant factor, then this constant should be introduced into the CFD simulation. If however the results vary inconsistently, it will confirm that further work is required on the CFD simulation. Possible methods of CFD improvement include continued mesh refinement, experimental testing to determine sand grain roughness for all surfaces and closer geometric modelling of the skirt deformation.

5.2 Skirt Design

From the conclusions drawn in this study, the air gap was found to be much lower than initially expected. In order to improve on this, further skirt refinement could be undertaken. One possible method of skirt refinement is to incorporate a series of ridges along the bottom of the where the skirt and ground contact. These ridges would act similar to a door seal and help reduce the effective air gap which would in turn increase the pressure under the skirt. By having a series of thin strips rather than a flat section, the friction between the skirt and the ground could be

significantly reduced. Eliminating this drag entirely may not be beneficial to the overall hoverboard design, as some drag is likely to provide stability for the rider.

5.3 Net Torque Concerns

5.3.1 Principle of Net Torque Rotation

One of the key issues with a blower and motor combination on an air cushion is the concept of net rotational torque. To get an object to move in straight line, or to deflect an object traveling in a straight line, it is necessary to apply a force. This is simply Newton's first law as stated by Hibbler (2007, pg 5). The same concept applies to start an object spinning, or to alter the rotation of a spinning object. As the motor and blower spin they will generate an inertia force. The only force resisting this inertia is the downward force exerted by the rider and the board, which is counter-acted by the pressure force providing lift, and the coefficient of friction between the air cushion and the board.

Given the limited coefficient of kinetic friction, given by Shan et al. (2008) as 0.0034, it can be assumed that this inertia generated by the blower and motor would be far greater than any friction resistance and therefore the board would rotate.

5.3.2 Overcoming Net Torque

The solutions for overcoming net torque are many and outside the scope of this project. Some potential methods for overcoming this issue have been presented here to encourage further development in this area.

Designing the motor and Blower so that they operated in opposite directions could potentially eliminate a large amount of net torque. For this to be successful the inertia of the two would need to be equal and opposite relative to the axis of rotation of the board. In addition to this friction effects between the air and the blower, and between the bearings and the motor would need to be compared. In order to achieve an opposite rotation, some method of reversing the direction between the motor and blower would be required. This could potentially be through a geared or pulley system, however each of these components takes up valuable space and adds weight and cost to the project.

An alternative is to use a dual motor and blower system that are counter-rotating. This would involve identical motors and blowers mounted at either end of the board. One motor/blower would rotate clockwise and the other would rotate counter-clockwise. These net torques would then cancel each other out to provide stability. An adjustment method for moving each motor towards the centre of the board could be implemented to allow for dynamic adjustments if the inertia of the two systems became unbalanced.

5.4 Blower Improvements

In this study only a single blower was experimentally tested for performance. It is envisioned that large amounts of research could be conducted into the area of blower optimisation.

An ideal blower would produce only the minimum required volumetric flow rate and pressure rise so as to reduce the power requirements of the batteries. In addition to this a small and lightweight design would enhance the marketability

of the final product. Preliminary research into blower design revealed that this is an extensive topic that would require a literature review of its own. As such it has been noted that it is a key area for improvement but no further investigation has been conducted.

Chapter 6

Conclusions

This section reviews the project specifications, the outcomes achieved in this study and how well these outcomes meet the specifications. It will discuss the methods used, the strengths and weaknesses of these methods and the potential impact this will have on the results. Finally this section concludes with the outcomes of the study in general and the limitations of the results.

6.1 Project objective 1

Project objective 1 as listed in the project specification was the:

Use Computational Fluid Dynamic (CFD) simulations to validate the results of experiments conducted by Shan et al. (2008). The purpose of this objective is to compare numerical CFD results with the experimental results conducted by Shan et al. (2008), and discuss any discrepancies.

It can be concluded that this project objective has been achieved as well as possible with the data provided by Shan et al. (2008). It is not possible to draw satisfactory

conclusions between the studies due the lack of input data provided by Shan et al. (2008), and the use of compressible flow without specifying what allowances were made for this in the study. The general trend that a higher number of air skirt outlet holes increased efficiency by reducing the pressure drop through the system has been confirmed.

6.2 Project objective 2

Project objective 2 as listed in the project specification was the:

Use CFD and Dimensionless Analysis to optimise the cushion outlet hole design for minimum energy losses by analysing pressure and velocity variations in different geometry. This objective will expand upon the research already done by Shan et al. (2008) and propose an optimum hole configuration for a specified pressure and air velocity value. The factors to be optimised are the number of holes, hole diameter, hole location and inlet velocity.

This objective has been achieved as relationships between the 4 key parameters have been established through the use of Pi Groups. Of these parameters, the number of holes was found to impact pressure loss the most. From the defined Pi Group relationships and the board geometry the parameters listed in Table 6-1 were selected as the optimum skirt configuration.

Parameter	Optimum Value
Outlet Hole Diameter D_1	0.009 m
Distance between hole centres D_2	0.135m
Number of Holes N	50
Inlet Velocity V	4.06 m/s

Table 6-1 Optimum values for specified parameters

These parameters fit the plots on the $N = 50$ curve for each Pi Group relationship and give the minimum pressure drop.

A limitation to the achievement of this objective is the lack of an experimental model to validate the CFD results against. Without this experimental test the CFD results remain unproven and cannot be reliably used to provide important data. If the experimental data confirms the CFD results then the Pi Group relationships created here can be applied to any simulation that is run under the same assumptions. The assumptions used in this model are that the system is in a steady state, flow is incompressible, kinetic and thermal energy losses are ignored and air behaves as an ideal gas.

6.3 Project objective 3

Project objective 2 as listed in the project specification was to:

Create a performance graph of the power source that is used for experimental testing. This is done experimentally to establish known values of static head, air velocity and power requirements for various volumetric flow rates of an Ozito OZBL 1800WA Leaf Blower. These values are then mapped on a performance graph so that optimum values can be selected. This optimum value is used in the CFD analysis and also in the experimental testing, to maintain consistency between the two.

This project objective was achieved successfully as outlined in section 3.1.3. A performance graph for a commercial leaf blower was created from accurate experimental test data. The benefits of this objective are that any further work

will have accurate information on which to base comparisons to this study and it will also allow for a comprehensive critical review of this study.

6.4 Project objective 4

Project objective 2 as listed in the project specification was to:

Build and test a prototype model using the validated power source. This objective aims to use experimental results in a controlled environment to either validate or disprove the CFD results. The Ozito OZBL 1800WA Leaf Blower will be used in the experimental testing and will have the same pressure and velocity inputs that were used in the CFD modelling.

This objective was not achieved due to the time constraints imposed on this study. In the initial project specification listed in Appendix A this objective was only to be completed if time permitted and was not the core focus of the study. The primary objective of this study was to create a CFD simulation model that could be compared to the results proposed by Shan et al. (2008).

6.5 Summary

This study effectively mapped the performance of a commercial leaf blower which was to be used as a power source in a novel hoverboard. These results were used in conjunction with Dimensional Analysis to create a set of Pi Groups which defined how the behaviour of 4 key parameters affected Pressure losses between the inlet and the cavity under the skirt. These Pi Group relationships were then

used to define the optimum board configuration for reducing pressure losses. Experimental validation of the CFD model was not achieved due to time restrictions placed on this study.

Further work to validate the CFD simulations is required before the Pi Group relationships and therefore the optimum configuration can be relied upon. The effects described in this study are limited to systems with the same skirt dimensions as listed in Appendix C and within the limits of the parameters that are shown in the Pi Group relationships.

References

Airlift Hovercraft, 2013, *Hovercraft Information*, Airlift Hovercraft, viewed 3rd June, 2014, <<http://airlifthovercraft.com/hovercraft-information/>>.

Amyot, JR, 1989, *Hovercraft Technology, Economics and Applications*, Elsevier Science Publishing Company Inc, New York.

ANSYS, 2012, *Introduction to ANSYS CFX – Lecture 04 Domains, Boundary Conditions and Sources*, version 14.5, program manual, ANSYS, Canonsburg.

ANSYS, 2009, *ANSYS CFX Solver Theory Guide*, release 12.1, program manual, ANSYS, Canonsburg.

Chen, M, Rong-de, L & Bang-jiao, Y, ‘Surface aerodynamic model of the lifter’, *Journal of Power Engineering*, Vol 71, Issue 2, pp 134-139.

Chung, J & Jung, T, ‘Optimisation of an air cushion vehicle bag and finger skirt using genetic algorithms’, *Journal of Aerospace and Technology*, Vol 8, 6th November 2003, pp 219-229.

Dixon, SL & Hall, CA 2010, *Fluid Mechanics and Thermodynamics of Turbomachinery*, 6th Edn, Elsevier Inc, New York.

Education Queensland, 2012, *Health and safety risk management*, Queensland Government, viewed 24th May, 2014, <<http://education.qld.gov.au/health/safety/managing/risk.html>>

Green, C, 2013, *Design: The Importance of Project Planning and Design in Moving toward Sustainability*, Engineers Australia, viewed 24th May, 2014, <<http://www.engineersaustralia.org.au/sites/default/files/shado/Representation/Policy%20Positions/Sustainability/Design.pdf>>.

Harrison, I, 2004, *The Book of Inventions*, National Geographic, Washington.

Hibbler, R. C, 2007, *Engineering Mechanics Statics*, 11th Edn, Pearson Prentice Hall, Singapore.

HobbyKing, 2014, *Electric Outrunner Motors (Online Catalogue)*, HobbyKing.com, viewed 17th May 2014, <http://hobbyking.com.au/hobbyking/store/_17986_Turnigy_RotoMax_1_60_Brushless_Outrunner_Motor.html>.

Kumar, E & Jerome, J, 'LQR based optimal tuning of PID controller for trajectory tracking of Magnetic Levitation System', *International Conference on Design and Manufacturing*, Vol 64, pp 254-264.

2014. *Maglev Trains: On Track with Superconductivity* [Online]. Available: <http://www.magnet.fsu.edu/education/tutorials/magnetacademy/superconductivity101/maglev.html> [Accessed 13th September 2014].

Mallove, EF, 2002, 'The "Lifter" Phenomenon: Electrogavitics, Antigravity, and more', *Infinite Energy*, Volume 8, Issue 45, viewed 17th May 2014, <<http://www.infinite-energy.com/iemagazine/issue45/thelifterphen.html>>.

Masuyama, K & Barrett, S, 'On the performance of electrohydrodynamic propulsion', *Proceedings of the Royal Society*, Vol 469, no. 2154, viewed 17th May 2014, <<http://rspa.royalsocietypublishing.org/content/469/2154/20120623.full.pdf+html>>.

Paxton Products, 2013, *XT Series Centrifugal Blowers (product specification sheet)*, Paxton Products, Viewed 16th May, 2014, <<http://www.paxtonproducts.com/Products/CentrifugalBlowers/tabid/88/Default.aspx>>.

Pritchard, P, 2011, *Fluid Mechanics*, 8th Edn, John Wiley & Sons, United States.

Radboud University, 2014, *Diamagnetic Levitation*, Radboud University Nijmegen, viewed 16th May, 2014, <http://www.ru.nl/hfml/research/levitation/diamagnetic/levitation_possible/>

Schmidt, C, 'Stability of superconductors in rapidly changing magnetic fields', *Cryogenics*, Vol. 30, Iss 6, pp 501-510.

Shan, Q, Yang, J, Chan, C, Zhang, G & Li, W, "Towards and Electric Powered Air-Gliding Skateboard", 2008 IEEE/ASME International Conference on Advanced Mechatronics, Chinese University of Hong Kong, Hong Kong.

Shanghai Maglev Transportation, 2005, *Maglev Technology*, Shanghai Maglev Transportation Development Co., Ltd, viewed 17th May 2014, <<http://www.smtdc.com/en/gycf3.html>>.

Shehadeh, M, Shennawy, Y, El-Gamal, H & Cheshire, D, *Similitude and scaling of Large Structural elements*, Alexandria University, Egypt, viewed 03rd June, 2014, <<http://www.fcet.staffs.ac.uk/dgc1/resources/journals/similitude.pdf>>.

Sleigh, P & Noakes, C, *An Introduction to Fluid Mechanics*, University of Leeds, England, viewed 14th October, 2014, <http://www.efm.leeds.ac.uk/CIVE/FluidsLevel1/Unit00/Downloads/Unit04-handout.pdf>.

Umicore, 2014, *Umicore Battery Recycling*, Umicore, viewed 24th May, 2014, <http://www.batteryrecycling.umicore.com/UBR/>.

Appendix A

Project Specification

PROJECT: Optimisation of an Air Gliding Skateboard

AUTHOR: Benjamin Allan John

KEYWORDS: Hoverboard, Hovercraft, Fluid Simulation, optimisation

ABSTRACT:

A Skateboard is a type of sporting equipment made of maplewood board approximately 16mm thick and two sets of wheels on which it rolls. The skateboard is generally propelled forward with one foot while the other remains on the board, or alternatively it can be used in skate parks and half pipes. Since the release of the 1985 movie "Back to the Future" the idea of a "hoverboard" has been entertained by people worldwide. This project aims to move toward the eventual development of a marketable and effective hoverboard using the concept of an air bearing to keep the rider elevated from the ground.

This project aims to validate the results of experiments conducted by Shan et al. (2008) for the development of a novel air-gliding (hovering) "skateboard". The results presented in the paper predict a co-efficient of static friction between the base of the board and the ground of 0.0088 and a co-efficient of kinetic friction of 0.0034. Further experiments determined that the optimum number of air outlet holes in the board was 44, as this reduced the standard deviation of the air outlet velocity to 3.7. These results are valid for the dimensions of the board listed in the paper using a conventional air blower.

Using the same dimensional parameters as the above mentioned paper, it is hoped that similar results can be obtained through fluid simulation. Using these as a baseline, the optimisation of air outlet holes will then be expanded upon to incorporate hole quantity, location, diameter, rider weight and inlet velocities. This will achieve a cushion design with consistent and stable outlet air velocities which will provide a stable platform.

A prototype will be designed using a 3-D modelling package based on the optimum design achieved from the fluid simulation.

If time permits:

- A prototype board will be manufactured and tested and the experimental results will be compared to the fluid simulation. This prototype board would be run from an aircompressor or general purpose leaf blower.

- The board will be designed so that a fan/power source are incorporated into the "deck" of the board rather than being supplied by an external device, and powered with either a Li-Po or Solar power source.

Shan, Q, Yang, J, Chan, C, Zhang, G & Li, W, "Towards and Electric Powered Air-Gliding Skateboard", 2008 IEEE/ASME International Conference on Advanced Mechatronics, Chinese University of Hong Kong, Hong Kong.

Appendix B

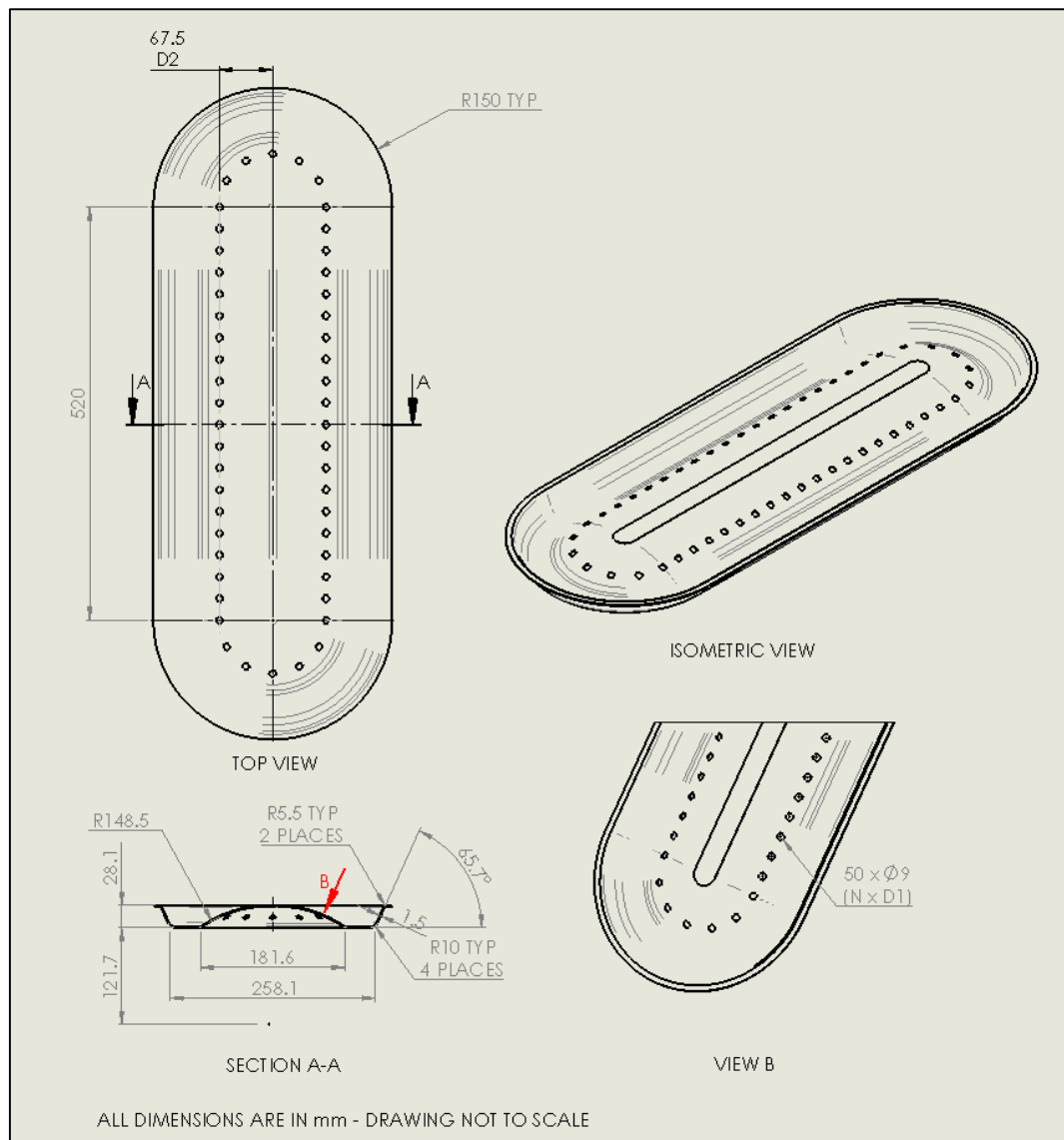
Pi Group Models

Model No.	D1 (mm)	D2 (mm)	N	P (Pa)	V (m/s)	Pi Group	Notes
1	8	100	30	170000	2.5	1	
2	8	100	40	170000	2.5	1	
3	8	100	50	170000	2.5	1	
4	8	110	30	170000	2.5	1	Re-use for Pi group 3
5	8	110	40	170000	2.5	1	Re-use for Pi group 3
6	8	110	50	170000	2.5	1	Re-use for Pi group 3
7	8	120	30	170000	2.5	1	
8	8	120	40	170000	2.5	1	
9	8	120	50	170000	2.5	1	
10	16	110	30	170000	2.0	Pi Group 2	
11	16	110	40	170000	2.0	Pi Group 2	
12	16	110	50	170000	2.0	Pi Group 2	
13	16	110	30	170000	2.5	Pi Group 2	Re-use for Pi group 3
14	16	110	40	170000	2.5	Pi Group 2	Re-use for Pi group 3
15	16	110	50	170000	2.5	Pi Group 2	Re-use for Pi group 3
16	16	110	30	170000	3.0	Pi Group 2	
17	16	110	40	170000	3.0	Pi Group 2	
18	16	110	50	170000	3.0	Pi Group 2	
19	24	110	30	170000	2.5	Pi Group 3	
20	24	110	40	170000	2.5	Pi Group 3	
21	24	110	50	170000	2.5	Pi Group 3	

Table B-1 Parameters for Simulation Models

Appendix C

Board Dimensions



Appendix D

FEA Reports

10/29/2014

ANSYS Report



Date

2014/10/29 16:31:24

Contents

[1. File Report](#)

[Table 1](#) File Information for Optimised 0.5mm gap

[2. Mesh Report](#)

[Table 2](#) Mesh Information for Optimised 0.5mm gap

[3. Physics Report](#)

[Table 3](#) Domain Physics for Optimised 0.5mm gap

[Table 4](#) Boundary Physics for Optimised 0.5mm gap

[4. User Data](#)

[Chart 1](#)

[Chart 2](#)

10/29/2014

ANSYS Report

1. File Report

Table 1. File Information for Optimised 0.5mm gap

Case	Optimised 0.5mm gap
File Path	F:\Final_3_files\dp0\CFX-20\CFX\CFX_001.res
File Date	29 October 2014
File Time	11:08:50 AM
File Type	CFX5
File Version	15.0

I:\SW\1\CFX_20\Hiss\Optimised\0.5mm\0.5gap.tlm

27

2. Mesh Report

Table 2. Mesh Information for Optimised 0.5mm gap

Domain	Nodes	Elements
Default Domain	82221	404823

10/29/2011

ANSYS Report

3. Physics Report

Table 3. Domain Physics for Optimised 0.5mm gap

Domain - Default Domain	
Type	Fluid
Location	B196
Materials	
Air Ideal Gas	
Fluid Definition	Material Library
Morphology	Continuous Fluid
Settings	
Buoyancy Model	Non Buoyant
Domain Motion	Stationary
Reference Pressure	1.0000e+00 [atm]
Heat Transfer Model	Isothermal
Fluid Temperature	2.5000e+01 [C]
Turbulence Model	k epsilon
Turbulent Wall Functions	Scalable

Table 4. Boundary Physics for Optimised 0.5mm gap

Domain	Boundaries	
Default Domain	Boundary - Inlet	
	Type	INLET
	Location	Inlet
	Settings	
	Flow Regime	Subsonic
	Mass And Momentum	Normal Speed
	Normal Speed	4.0600e+00 [m s ⁻¹]
	Turbulence	High Intensity and Eddy Viscosity Ratio
	Boundary - Outlet	
	Type	OUTLET
	Location	Outlet
	Settings	
	Flow Regime	Subsonic
	Mass And Momentum	Static Pressure
	Relative	0.0000e+00 [Pa]

file:///C:/Users/20110105/Desktop/200.5mm%20gap.tn

27

10283371

ANSYS Raxx1

Pressure	
Boundary - Symmetry	
Type	SYMMETRY
Location	Symmetry
<i>Settings</i>	
Boundary - Symmetry2	
Type	SYMMETRY
Location	Symmetry2
<i>Settings</i>	
Boundary - Air Gap	
Type	WALL
Location	AirGap
<i>Settings</i>	
Mass And Momentum	No Slip Wall
Wall Roughness	Rough Wall
Sand Grain Roughness Height	2.5000e-01 [mm]
Boundary - Default Domain Default	
Type	WALL
Location	F179.196, F180.196, F181.196, F182.196, F183.196, F184.196, F185.196, F186.196, F187.196, F188.196, F189.196, F190.196, F191.196, F192.196, F197.196, F198.196, F199.196, F200.196, F201.196, F202.196, F203.196, F204.196, F205.196, F206.196, F207.196, F208.196, F209.196, F210.196, F212.196, F213.196, F214.196, F215.196, F216.196, F217.196, F218.196, F221.196, F222.196, F223.196, F224.196, F225.196, F226.196, F227.196, F228.196, F229.196, F230.196, F231.196, F232.196, F235.196, F236.196, F237.196, F238.196, F239.196, F240.196, F241.196, F244.196
<i>Settings</i>	
Mass And Momentum	No Slip Wall
Wall Roughness	Smooth Wall
Boundary - Ground	
Type	WALL
Location	Ground
<i>Settings</i>	
Mass And	No Slip Wall

1162711-CH-2-420115-001nsd/200.0mm/420gap.tlm

57

10/28/2011

ANSYS Raptor

4. User Data

Chart 1.

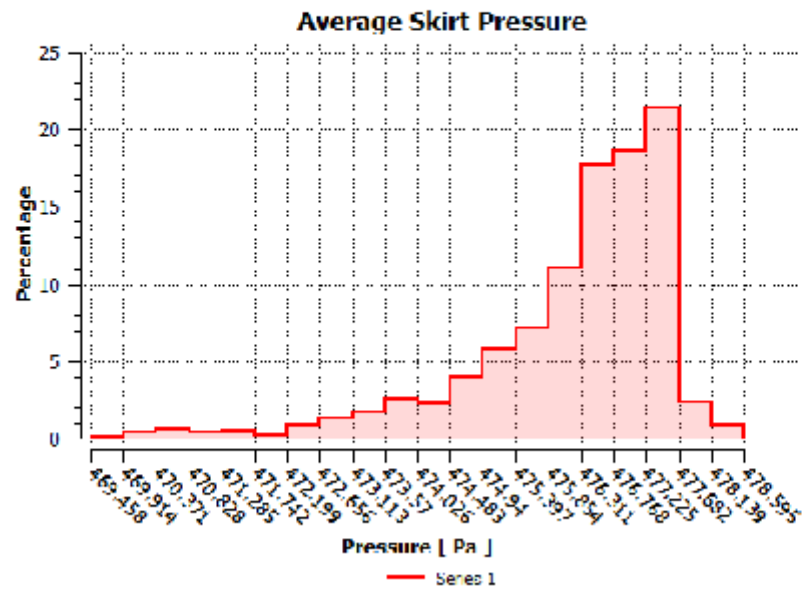
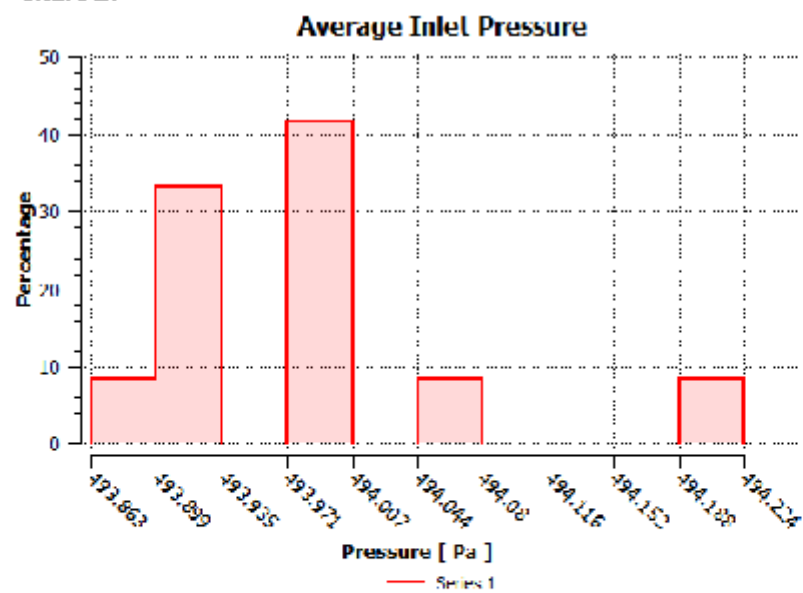


Chart 2.

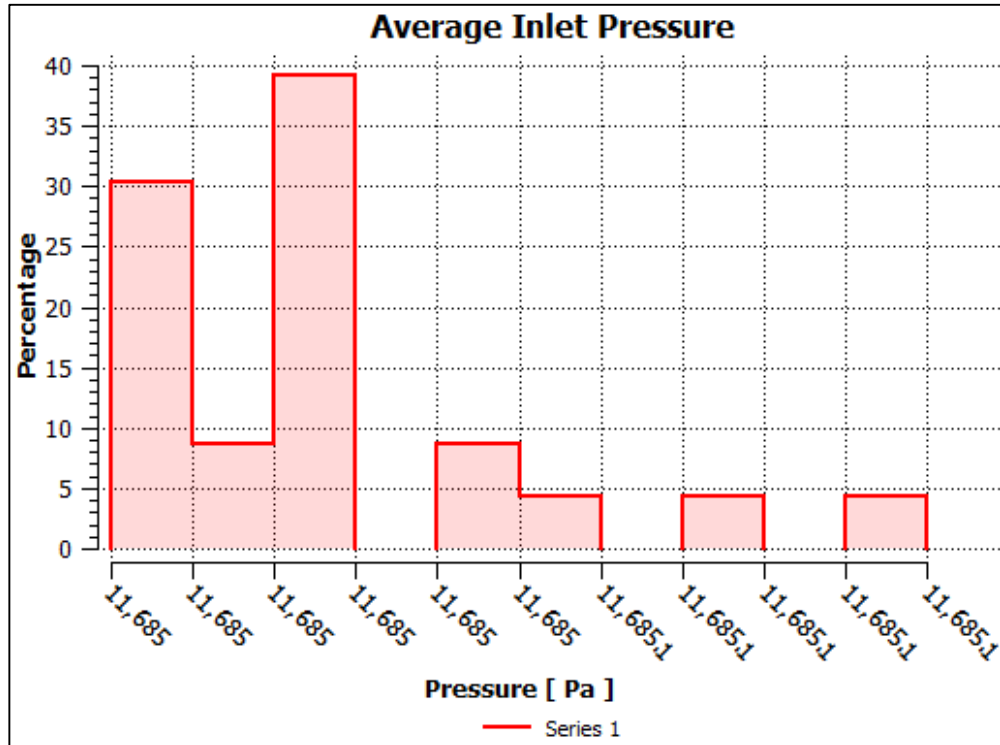
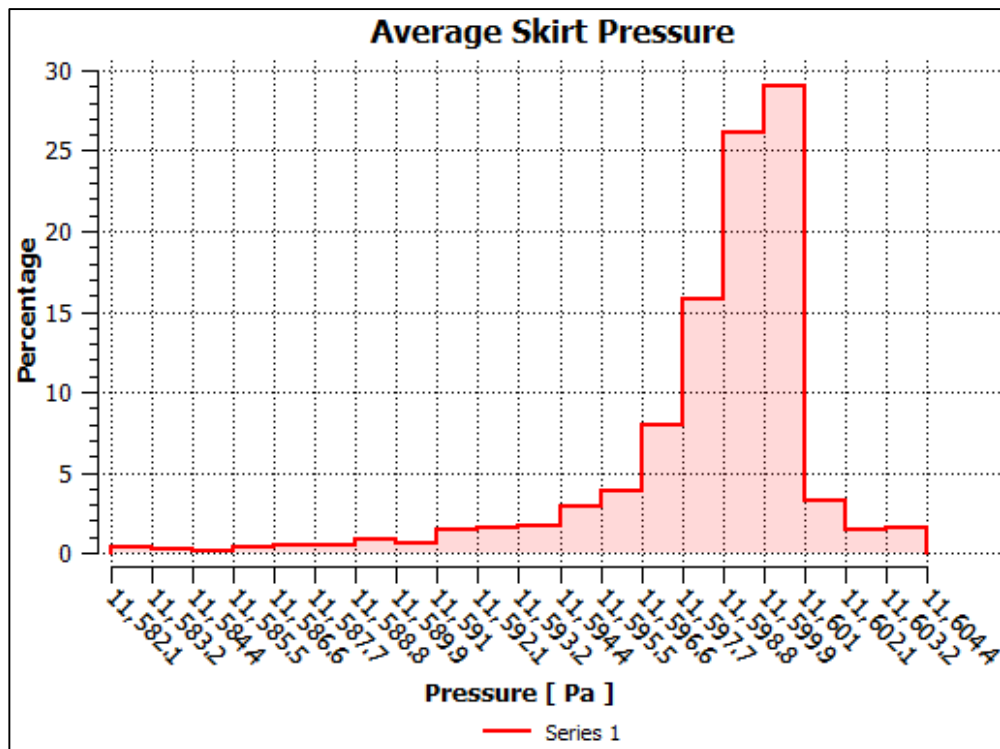


10/29/2011

ANSYS Report

Momentum	
Wall Roughness	Rough Wall
Sand Grain Roughness Height	5.0000e-01 [mm]
Boundary - Skirt Pressure	
Type	WALL
Location	SkirtPressure
<i>Settings</i>	
Mass And Momentum	No Slip Wall
Wall Roughness	Rough Wall
Sand Grain Roughness Height	2.5000e-01 [mm]
Boundary - Top	
Type	WALL
Location	Top
<i>Settings</i>	
Mass And Momentum	Free Slip Wall

SAMPLE SIMULATION HISTOGRAM PLOTS (SIMULATION 1)



Appendix E

Risk Assessment

value wellbeing lead people active support

Health & Safety Risk Assessment Template


Use this template to document a risk assessment to manage health and safety hazards and risks.
For more details on the risk management process refer to: [Managing Health and Safety Risks](#).
Note: For risk assessments with curriculum activities refer to: [Managing Risks in School Curriculum Activities](#).

Activity Description: Build and Test Prototype Hoverboard

Conducted by: Benjamin John Date:

Step 1: Identify the Hazards

Biological (e.g. hygiene, disease, infection)		
<input type="checkbox"/> Blood / Bodily fluid	<input type="checkbox"/> Virus / Disease	<input type="checkbox"/> Food handling
Other/Details: <u>Nil</u>		
Chemicals Note: Refer to the label and Safety Data Sheet (SDS) for the classification and management of all chemicals.		
<input type="checkbox"/> Non-hazardous chemical(s)	<input type="checkbox"/> 'Hazardous' chemical (Refer to a completed hazardous chemical risk assessment)	
Name of chemical(s) / Details: <u>Nil</u>		
Critical Incident – resulting in:		
<input type="checkbox"/> Lockdown	<input type="checkbox"/> Evacuation	<input checked="" type="checkbox"/> Disruption
Other/Details: <u> </u>		
Energy Systems – Incident / Issues involving:		
<input checked="" type="checkbox"/> Electricity (incl. Mains and Solar)	<input type="checkbox"/> LPG Gas	<input checked="" type="checkbox"/> Gas / Pressurised containers
Other/Details: <u> </u>		
Environment		
<input type="checkbox"/> Sun exposure	<input type="checkbox"/> Water (creek, river, beach, dam)	<input checked="" type="checkbox"/> Sound / Noise
<input type="checkbox"/> Animals / Insects	<input type="checkbox"/> Storms / Weather	<input type="checkbox"/> Temperature (heat, cold)
Other/Details: <u> </u>		
Facilities / Built Environment		
<input type="checkbox"/> Buildings and fixtures	<input type="checkbox"/> Driveway / Paths	<input checked="" type="checkbox"/> Workshops / Work rooms
<input type="checkbox"/> Playground equipment	<input type="checkbox"/> Furniture	<input type="checkbox"/> Swimming pool
Other/Details: <u> </u>		
Machinery, Plant and Equipment		
<input type="checkbox"/> Machinery (fixed plant)	<input type="checkbox"/> Machinery (portable)	<input checked="" type="checkbox"/> Hand tools
<input type="checkbox"/> Vehicles / trailers		
Other/Details: <u> </u>		
Manual Tasks / Ergonomics		
<input type="checkbox"/> Manual tasks (repetitive, heavy)	<input type="checkbox"/> Working at heights	<input type="checkbox"/> Restricted space
Other/Details: <u> </u>		
People		
<input type="checkbox"/> Students	<input type="checkbox"/> Staff	<input type="checkbox"/> Parents / Others
<input checked="" type="checkbox"/> Physical	<input type="checkbox"/> Psychological / Stress	
Other/Details: <u> </u>		
Other Hazards / Details		
<p>There will be cutting/injury hazards associated with using power tools and hand tools to craft the board and construct it. There will be the risk of high velocity compressed air associated with the electric Leaf Blower when testing the board. There will also be electricity hazards as the leaf blower is powered by 240V electrical supply.</p>		



Organisational Health
Department of Education, Training and Employment

Issued: August 2012
Uncontrolled when printed

Page 1 of 4

Step 2: Assess the Level of Risk

Consider the hazards identified in Step One and use the risk assessment matrix below as a guide to assess the risk level.

Likelihood	Consequence				
	Insignificant	Minor	Moderate	Major	Critical
Almost Certain	Medium	Medium	High	Extreme	Extreme
Likely	Low	Medium	High	High	Extreme
Possible	Low	Medium	High	High	High
Unlikely	Low	Low	Medium	Medium	High
Rare	Low	Low	Low	Low	Medium


Consequence	Description of Consequence	Likelihood	Description of Likelihood
1. Insignificant	No treatment required	1. Rare	Will only occur in exceptional circumstances
2. Minor	Minor injury requiring First Aid treatment (e.g. minor cuts, bruises, bumps)	2. Unlikely	Not likely to occur within the foreseeable future, or within the project lifecycle
3. Moderate	Injury requiring medical treatment or lost time	3. Possible	May occur within the foreseeable future, or within the project lifecycle
4. Major	Serious injury (injuries) requiring specialist medical treatment or hospitalisation	4. Likely	Likely to occur within the foreseeable future, or within the project lifecycle
5. Critical	Loss of life, permanent disability or multiple serious injuries	5. Almost Certain	Almost certain to occur within the foreseeable future or within the project lifecycle

Assessed Risk Level	Description of Risk Level	Actions
<input type="checkbox"/> Low	If an incident were to occur, there would be little likelihood that an injury would result.	Undertake the activity with the existing controls in place.
<input checked="" type="checkbox"/> Medium	If an incident were to occur, there would be some chance that an injury requiring First Aid would result.	Additional controls may be needed.
<input type="checkbox"/> High	If an incident were to occur, it would be likely that an injury requiring medical treatment would result.	Controls will need to be in place before the activity is undertaken.
<input type="checkbox"/> Extreme	If an incident were to occur, it would be likely that a permanent, debilitating injury or death would result.	Consider alternatives to doing the activity. Significant control measures will need to be implemented to ensure safety.

Step 3: Control the Risk

In the table below:

- List below the hazards/risks you identified in Step One.
 - Rate their risk level (refer to information contained in Step Two to assist with this).
 - Detail the control measures you will implement to eliminate or minimise the risk.
- Note: Control measures should be implemented in accordance with the preferred **hierarchy of control**. If lower level controls (such as Administration or PPE) are to be implemented without higher level controls, it is important that the reasons are explained.

Hierarchy of Control	
Most effective (High level)  Least effective (Low level)	Elimination: remove the hazard completely from the workplace or activity
	Substitution: replace a hazard with a less dangerous one (e.g. a less hazardous chemical)
	Redesign: making a machine or work process safer (e.g. raise a bench to reduce bending)
	Isolation: separate people from the hazard (e.g. safety barrier)
	Administration: putting rules, signage or training in place to make a workplace safer (e.g. induction training, highlighting trip hazards)
	Personal Protective Equipment (PPE): Protective clothing and equipment (e.g. gloves, hats)



Hazards/Risks and Control Measures

1. Description of Hazards / Risks	2. Risk Level	4. Control Measures (Note: If only Administration or PPE controls are used, please explain why.)
Using hand tools to build Hoverboard - Risk of cuts, physical injury, electrical injury.	Medium	Trade qualified operator to use all tools. Wear all appropriate PPE for the necessary tools. Work in pairs so that if injury occurs medical treatment can be administered.
Testing Hoverboard - Flying particles, compressed air	Medium	Ensure all compressed air lines between the leaf blower and the test board are connected before using the blower. Maintain 1m clearance from the base of the board at all times. Wear PPE including long clothes, gloves, safety glasses.
Electrical Shock	High	Ensure all electrical equipment has a current test and tag inspection label. Conduct a visual inspection of the electrical cord before use.
Other details:		